Gadolinium Vanadate Nanocrystals as Carriers of α-Emitters (^{225}Ac, ^{227}Th) and Contrast Agents

Miguel Toro-González[ab], Ashley N. Dame[b], Saed Mirzadeh[b], Jessika V. Rojas[a*]

[a] Department of Mechanical and Nuclear Engineering, Virginia Commonwealth University, Richmond, VA, United States. E-mail: torogonzalezm@vcu.edu (Miguel Toro-González), jvrojas@vcu.edu (Jessika V. Rojas).
[b] Isotope and Fuel Cycle Technology Division, Oak Ridge National Laboratory, Oak Ridge, TN, United States. E-mail: torogonzalmt@ornl.gov (Miguel Toro-González), damean@ornl.gov (Ashley N. Dame), mirzadehs@ornl.gov (Saed Mirzadeh).
*Corresponding author: Jessika V. Rojas, jvrojas@vcu.edu, (804) 828-4267
ORCID: Miguel Toro-González (0000-0003-3320-423X), Ashley N. Dame (0000-0002-9577-5006), Saed Mirzadeh (0000-0002-1774-7958), Jessika V. Rojas (0000-0002-2268-4613)

Abstract

Gadolinium vanadate ($GdVO_4$) core and core + 2 shells nanocrystals (NCs) were evaluated for *in vitro* retention of ^{225}Ac, ^{227}Th, and their first decay daughters, ^{221}Fr and ^{223}Ra, respectively. $GdVO_4$ NCs with a tetragonal crystal system (zircon-type) and spherical morphology were obtained by precipitation of $GdCl_3$ and Na_3VO_4 using sodium citrate as complexing agent. Growth of two nonradioactive $GdVO_4$ shells on both Gd(^{225}Ac)VO_4 and Gd(^{227}Th)VO_4 core NCs was demonstrated by an increase of 0.7 nm and 2 nm in the crystallite size, respectively. The maximum leakage of ^{225}Ac was 15% and 2.4% from core and core + 2 shells, whereas the leakage of ^{227}Th was 3% and 1.5%, respectively. The presence of two nonradioactive $GdVO_4$ shells increased the retention of ^{221}Fr and ^{223}Ra by 20% and 15% with respect to core NCs. Further, a longitudinal proton relaxivity, $r_1 = 0.9289\ s^{-1}\ mM^{-1}$, confirmed their potential application as contrast agents for magnetic resonance imaging. In summary, $GdVO_4$ NCs show promising capabilities as radionuclide carriers with partial retention of decay daughters and as contrast agents for theranostic applications.

Keywords

Actinium-225, thorium-227, radionuclide retention, multifunctional nanocrystals, gadolinium vanadate

Introduction

Lanthanide-based nanomaterials are among various inorganic compounds with potential application in nanomedicine for diagnosis and treatment of multiple diseases.[1] The unique optical and magnetic properties of Ln cations provide functionalities for multimodal molecular imaging.[1,2] Changes in the elemental composition and concentration of Ln cations can result in either downshifting, downconversion, or upconversion luminescence. The latter is preferable for *in vivo* biomedical applications because of the large penetration depth of infrared light in tissue and minimal photodamage to cells.[3] The shielding of the 4*f* electrons by the 5*s* and 5*p* orbitals in the ground state electronic configuration of Ln cations ($4f^n$, n = 0 − 14) results in excellent photostability, long luminescence lifetimes, narrow emission bands, and large Stoke/anti-Stoke shifts, among others.[1,3–5] The strong unquenched angular momentum of the 4*f* electrons induces effective spin-orbit coupling and paramagnetic properties to Ln cations.[4] These paramagnetic properties have been exploited in commercial magnetic resonance imaging (MRI) contrast agents such as Magnevist®, Omniscan, and OptiMARK, which consist of a Gd^{3+} ion complexed with a chelating ligand.[6] Lastly, the high atomic number of Ln cations makes them suitable as contrast agents for x-ray computed tomography.[7,8]

Among Ln-based nanomaterials, gadolinium vanadate ($GdVO_4$) exhibits multiple characteristics that make it attractive for biomedical applications. First, multiple studies have demonstrated that $GdVO_4$ can be easily doped for the development of down-conversion[9–14] or up-conversion[15–18] nanomaterials because of the similarity between the ionic radii of Ln cations. Second, $GdVO_4$ nanomaterials could provide a higher contrast in MRI with respect to Gd-chelates because of the large quantity of Gd^{3+} ions contained within a single carrier.[4] The toxicity related to the dissociation of Gd^{3+} ions from Gd-chelates, caused by the transmetallation with endogenous cations, is reduced in $GdVO_4$ because the Gd cations bound within the inorganic crystal lattice are not accessible to transmetallation.[4,6] Third, $GdVO_4$ nanomaterials can combine the luminescence and magnetic properties of Ln cations within a single platform for multimodal molecular imaging.[9,10,15] Eu-doped $GdVO_4$ nanomaterials have shown capabilities as contrast agents for fluorescence imaging and MRI, with higher longitudinal (r_1) proton relaxivity than that of pure $GdVO_4$.[11,19] Finally, the negligible toxicity effects revealed by Ln-doped $GdVO_4$ nanomaterials supports their use as multifunctional platforms for *in vivo* biomedical applications.[9,11]

Photodynamic therapy, radiation therapy, and drug delivery are among potential applications of $GdVO_4$ nanomaterials.[2,4] The drug delivery capabilities of Eu-doped $GdVO_4$ nanoparticles (NPs) coated with mesoporous silica were tested using the chemotherapeutic agent Doxorubicin.[10] Recent interest has also focused on using Ln-based nanomaterials as carriers of therapeutically relevant β- and α-emitting radionuclides.[20–27] *In vivo* α-generators such as ^{225}Ac, ^{227}Th, and ^{223}Ra have been proposed for treatment of disseminated cancer cells and micrometastases because of the high linear energy transfer and relative biological effectiveness of α-particles.[28–32] The main challenge of using these radionuclides, with a number of radioactive members in their decay chain, involves the retention of decay daughters at the target site to

prevent global toxicity to healthy organs and to improve treatment efficacy by maintaining very high local toxicity.[28] The retention of radionuclides at the target site may be affected by the *in vivo* stability of the carrier, the resistance to radiation damage of the carrier, and the highly energetic daughter nucleus that is generated upon decay.[33] Lanthanide phosphate NPs have been proven to enhance the retention of *in vivo* α-generators and decay daughters and their radiochemical yield compared to that of alternative carriers such as radioimmunoconjugates or polymersomes.[20,22] For example, a 41.1% and 18.7% of free ^{213}Bi and ^{221}Fr were found in the kidney after *in vivo* biodistribution studies using ^{225}Ac-labeled anti-rat HER-2/*neu* mAb, which displayed only 12% ^{225}Ac labeling efficiency.[34] Polymersomes of 200 nm had a loading efficiency ~67% for ^{225}Ac, whereas the retention of its first decay daughter ^{221}Fr was ~50%.[35] $LaPO_4$ core NPs (3–5 nm) doped with ^{225}Ac had a 66% ^{225}Ac radiochemical yield and a 40% retention of ^{221}Fr over 30 days.[20] $LnPO_4$ core-shell NPs, having four shells of $GdPO_4$ and a gold layer, enhanced the radiochemical yield of ^{225}Ac and retention of ^{221}Fr up to ~76% and ~91%, respectively.[22] A 91% ^{223}Ra radiochemical yield was obtained for $LaPO_4$ core + 2 shells NPs doped with ^{223}Ra, whereas the retention of decay daughter ^{211}Pb was quantitative (~100%).[23] The successful retention of ^{223}Ra and its decay daughters is of utmost importance because of the lack of stable complexing agents for radium isotopes, which has restricted their implementation in radioimmunotherapy.[36] In summary, Ln-based NPs have shown potential application as *in vivo* therapeutic platforms, particularly for targeted alpha therapy, based on their capacity to retain radionuclides, modify their surface with functional groups and antibodies, and increase the specific activity within the carrier without causing detrimental effects to the radiochemical yield.[20]

In this work, $GdVO_4$ core–shell nanocrystals (NCs) were synthesized by precipitation of Gd^{3+} and $[VO_4]^{3-}$ ions in the presence of sodium citrate, as complexing agent. The concentration between precursors was varied to optimize the chemical yield and increase the particle size and shell thickness. The crystal structure, morphology, particle size distribution, chemical yield, and response as MRI contrast agent of $GdVO_4$ NCs were assessed. $GdVO_4$ core–shell NCs containing α-emitters ^{225}Ac and ^{227}Th were synthesized to evaluate their radiochemical yield and *in vitro* retention of their first decay daughters ^{221}Fr and ^{223}Ra, respectively. It is expected that the zircon structure of $LnVO_4$ compounds will provide comparable retention capabilities to those of $LnPO_4$ NPs based on their resistance to radiation damage.[37] The synthesis and characterization of NPs doped with ^{227}Th has not been reported, whereas previous studies have only involved the development of ^{227}Th radioimmunoconjugates that cannot retain decay daughters at the target site.[28,30,36,38–43] The partial retention of decay daughters within $GdVO_4$ NCs will help minimize the radiotoxicity and promote the use of ^{227}Th for therapeutic purposes.[43] Additionally, the generation of ^{227}Th from thermal neutron irradiation of a ^{226}Ra target will allow its production in clinically relevant quantities.[36,44]

Materials and Methods

Synthesis of $GdVO_4$ core–shell NCs

A four-step chemical process, consisting in both anion and cation exchange chromatography, was used to obtain carrier-free ^{225}Ac from a thorium stock consisting of ^{228}Th, ^{229}Th, and ^{232}Th.[45] Thorium-227 was obtained from actinium-227 ($T_{1/2}$ = 21.7 years) generated via thermal neutron irradiation of a radium-226 target. Recovery of carrier-free ^{227}Th for synthesis purposes was achieved through anion exchange chromatography. Both ^{225}Ac and ^{227}Th were prepared at Oak Ridge National Laboratory. $GdVO_4$ core and core + 2 shells NCs were synthesized following an aqueous route based on the precipitation of gadolinium cations and orthovanadate anions in the presence of sodium citrate as complexing agent.[46] The aqueous solutions were prepared with deionized (DI) water (18 MΩ) obtained from a MilliQ® water purification system. Gadolinium(III) chloride hexahydrate ($GdCl_3 \cdot 6H_2O$, 99.9%, trace metal basis, Sigma Aldrich), sodium citrate dihydrate ($Na_3C_6H_5O_7 \cdot 2H_2O$, ultrapure bioreagent, Sigma Aldrich), and sodium orthovanadate (Na_3VO_4, 99%, Acros Organics) were prepared at a concentration of 0.1 M in DI water. The pH of Na_3VO_4 was adjusted to 12.5 using NaOH (1 M) before synthesis.

Huignard *et al*. proposed a 1:0.75:0.75 volume ratio between Ln:Cit:VO_4 for the synthesis of europium-doped YVO_4 NPs.[46] This exact volume ratio was implemented for the synthesis Gd(^{225}Ac)VO_4 core–shell NCs. Preparation of Gd(^{225}Ac)VO_4 core NCs began by transferring ~50 µCi of ^{225}Ac on an acidic media into a conical vial. The radioactive solution was evaporated to dryness at 80ºC. Afterward, a solution of $GdCl_3$ was added and stirred for 10–15 minutes to ensure a homogeneous mixture. A 0.75 volume equivalent of sodium citrate dihydrate was added drop-by-drop to the conical vial under constant stirring. The interaction between ^{225}Ac/Gd and citrate ions resulted in the formation of a white turbid suspension containing ^{225}Ac/Gd-Cit complexes. A translucent solution was obtained after adding 0.75 volume equivalent of Na_3VO_4 under constant stirring. This mixture containing ^{225}Ac/Gd-Cit-VO_4 oligomeric species was heated at 60ºC for 30 minutes under constant stirring to synthesize Gd(^{225}Ac)VO_4 core NCs. The synthesized core NCs were allowed to cool down followed by either the deposition of $GdVO_4$ shells or dialysis against DI water to assess the *in vitro* retention of radionuclides. Dialysis was performed using a Biotech regenerated cellulose membrane with an 8–10 kDa molecular weight cut-off purchased from Spectrum Labs® (Repligen Corporation, Waltham, MA). The membrane was washed several times with DI water before use to remove preservatives. The synthesis of core–shell NCs consisted of mixing the radioactive core NCs suspension with a solution containing Gd-Cit-VO_4 oligomeric species, prepared as described previously, in a 1:1.5 volume ratio under constant stirring. This mixture was heated at 60ºC for 30 minutes under constant stirring to synthesize $GdVO_4$ core + 1 shell NCs. This process was repeated once more, keeping the volume ratio between core NCs suspension and oligomeric species solution at 1:1.5, for the deposition of two $GdVO_4$ shells on Gd(^{225}Ac)VO_4 core NCs. The as-prepared Gd(^{225}Ac)VO_4 core + 2 shells were dialyzed against DI water to remove unreacted species and evaluate the *in vitro* retention of ^{225}Ac and its first decay daughter, ^{221}Fr.

Gd(^{227}Th)VO_4 core–shell NCs were synthesized using a 1:0.65:0.9 volume ratio between Gd:Cit:VO_4. This modification was done to enhance the NC's chemical yield and to increase the shell thickness. An acidic solution with an initial activity of ~32 µCi of ^{227}Th was evaporated to dryness in a conical vial at 80ºC. A $GdCl_3$ solution was added to the vial and stirred for 10–15 minutes for a complete dispersion of ^{227}Th and decay daughters in solution. Sodium citrate and sodium orthovanadate solutions were added drop-by-drop under constant stirring at the established volume ratios. Gd(^{227}Th)VO_4 core NCs were obtained after heating the solution containing ^{227}Th/Gd-Cit-VO_4 oligomeric species at 60ºC for 30 minutes. The radioactive core suspension was transferred into the regenerated cellulose membrane for dialysis overnight. After dialysis, the core solution was divided into two equal parts, one for retention studies and the other for core–shell synthesis. The growth of $GdVO_4$ shells was completed using the dialyzed Gd(^{227}Th)VO_4 core NCs suspension to prevent the deposition of unreacted ^{227}Th and decay daughters. Non-radioactive shells were deposited by mixing the dialyzed core NCs suspension with a solution containing Gd-Cit-VO_4 oligomeric species using the same volume ratio previously described. A 1:2 volume ratio between radioactive core NCs suspension and oligomeric species solution was used for the deposition of a thick nonradioactive $GdVO_4$ shell. This mixture was subsequently heated at 60ºC for 30 minutes to deposit the first shell. The process was repeated once more to synthesize Gd(^{227}Th)VO_4 core + 2 shells NCs, while keeping a 1:2 volume ratio of core NCs suspension to Gd-Cit-VO_4 oligomeric species solution. The core + 2 shells NCs suspension was dialyzed against DI water to assess *in vitro* retention of ^{227}Th and its first decay daughter, ^{223}Ra. Nonradioactive $GdVO_4$ core and core + 2 shells NCs were synthesized following the procedures described above for ^{225}Ac and ^{227}Th and are designated herein as $GdVO_4$-Ac and $GdVO_4$-Th, respectively. The following nomenclature has also been used to facilitate identification of the radioactive samples: Gd(isotope)VO_4 and Gd(isotope)VO_4/2$GdVO_4$ for core and core + 2 shells NCs, respectively.

Characterization

Nonradioactive $GdVO_4$ NCs were prepared under identical conditions and characterized. The crystal structure of $GdVO_4$ core and core + 2 shells NCs was determined by x-ray diffraction using a PANanalytical X'Pert Pro MPD x-ray diffractometer. The diffractometer was operated at 45 kV and 40 mA with a Cu anode (Cu k_α, λ = 1.504 Å). The powder samples were obtained by mixing the as-prepared $GdVO_4$ core and core + 2 shells NCs suspensions with ethanol and precipitating them using centrifugation. The precipitates were dried at 60ºC for 18 hours in an oven and then ground using a mortar and pestle until fine powders were obtained. The morphology of the NCs was assessed using transmission electron microscopy in a FEI Titan and a NEOARM JEOL operating at accelerating voltages of 300 kV and 60 kV, respectively. The sample preparation consisted in drop-casting as-prepared core and core + 2 shells NCs suspensions onto either a 300 mesh formvar/carbon or a 200 mesh Lacey carbon copper grid. The hydrodynamic size of the as-prepared NCs suspensions was evaluated using dynamic light scattering on a NanoPlus HD (Micromeritics®). This equipment uses a laser diode operated at

30 mW and 660 nm wavelength. Both intensity and number distributions were obtained for each sample. The zeta potential (ζ-potential) of as-prepared NCs suspensions was characterized using the zeta potential analyzer ZetaPALS (Brookhaven Instruments Corporation). Chemical yield of $GdVO_4$ core NCs was determined by inductively coupled plasma–optical emission spectroscopy (ICP-OES) on an Agilent 5110 ICP-OES. To assess the response as MRI contrast agents, phantom studies were completed to quantify the longitudinal relaxivity (r_1) induced by $GdVO_4$-Ac core NCs. The phantoms were prepared by diluting a dialyzed core NCs suspension at various concentrations (0.016–0.5 mM). Each solution was loaded into a 2 mL plastic syringe, avoiding air bubbles. The phantoms were imaged in a 7T BioSpec 70/30 small animal MRI scanner (Bruker, Billerica, MA). T_1 values and T_1-weighted images were obtained using the same multi-slice and multi-echo sequence. Longitudinal relaxivity (r_1) was obtained from the slope of the curve $1/T_1$ versus the Gd concentration expressed in millimoles.

Radiochemical yield and in vitro retention

The activity of ^{227}Th ($T_{1/2}$ = 18.7 days), ^{225}Ac ($T_{1/2}$ = 9.9 days), ^{223}Ra ($T_{1/2}$ = 11.4 days), and ^{221}Fr ($T_{1/2}$ = 4.9 minutes) was measured by γ-ray spectroscopy using a high-purity germanium (HPGe) detector (Ortec, Oak Ridge, TN) with a crystal active volume ~100 cm^3 and a Be window coupled to a PC-based multichannel analyzer (Canberra Industries, Meriden, CT). Energy and efficiency calibrations were determined by γ-ray sources traceable to the National Institute of Standards and Technology. Radiochemical yield and radionuclide retention were evaluated *in vitro* using a similar setup as reported previously for $LnPO_4$ NPs.[20,22,23] The initial activity of Gd(^{227}Th)VO_4, Gd(^{225}Ac)VO_4, Gd(^{227}Th)VO_4/2$GdVO_4$, and Gd(^{225}Ac)VO_4/2$GdVO_4$ was determined from an aliquot collected from the as-prepared suspensions. The glass conical vial, spin vane, and pipette tip used during synthesis were also assayed to determine the activity lost in the process. After synthesis, a 5 mL dialysate aliquot was analyzed to quantify the activity associated with unreacted radionuclides. Afterward, the dialysate was changed with clean DI, and radionuclide retention was evaluated periodically by taking 5 mL aliquots and measuring their activity in the HPGe detector. Because of the short half-life of ^{221}Fr, the time between the removal of the aliquot and the beginning of the counting was recorded for each sample. The assay of each aliquot from Gd(^{225}Ac)VO_4 and Gd(^{225}Ac)VO_4/2$GdVO_4$ consisted in 20 consecutive 1-minute interval measurements that were used to build a decay curve of ^{221}Fr. This same aliquot was counted the next day to determine the activity related to ^{225}Ac based on the activity of ^{221}Fr now in secular equilibrium. The γ-energy and intensities used for the evaluation of the activity from ^{221}Fr, ^{223}Ra, and ^{227}Th were 218 keV (11.4%), 269.4 keV (13.9%), and 236 keV (12.9%), respectively. The activity was corrected by attributing for the volume loss due to the aliquots withdrawn and radioactive decay.

Results and Discussion

Synthesis of $GdVO_4$ core–shell NCs

The synthesis of $GdVO_4$ core and core + 2 shells NCs was performed following an aqueous route based on the precipitation of Gd^{3+} and $[VO_4]^{3-}$ ions using sodium citrate as complexing agent [46]. The formation of $GdVO_4$ core NCs begins with Gd or Gd/actinide cations in solution. These cations interact with citrate ions to form Gd-Cit species, which changed the solution appearance from clear to turbid. The addition of sodium orthovanadate to the Gd-Cit solution results in Gd-Cit-VO_4 oligomeric species, while some $[VO_4]^{3-}$ species remain in solution. The heating of this mixture promotes the consumption of the oligomeric species allowing the interaction between Gd^{3+} and $[VO_4]^{3-}$ ions. The interaction between both ions results in the formation of $GdVO_4$ nuclei, which upon continuous heating grow to form $GdVO_4$ core NCs. These NCs are stabilized by citrate groups through complexation with surface Gd^{3+} ions.[46] The stabilization mechanism requires an excess of Gd^{3+} with respect to $[VO_4]^{3-}$ during the synthesis. Hence, the ratio of Gd^{3+} to $[VO_4]^{3-}$ used during the synthesis of Gd(^{225}Ac)VO_4 and Gd(^{227}Th)VO_4 core–shell NCs was 1:0.75 and 1:0.9, respectively. Gd(^{227}Th)VO_4 core–shell NCs are expected to have a broader particle size distribution with respect to Gd(^{225}Ac)VO_4 since the excess of Gd^{3+} ions and the concentration of sodium citrate are lower.

The development of core–shell structures is intended to increase the retention of parent radionuclide and decay daughters with respect to core NCs as has been reported previously.[22,23] The dense lattice structure of the shells will serve as a barrier to retain the decay daughters within the NCs, which is extremely important to prevent the release of radionuclides that can deliver unwanted dose to healthy tissue. Core–shell NCs were synthesized by mixing the core NCs suspensions with a mixture containing Gd-Cit-VO_4 oligomeric species. Upon heating, the oligomeric species are consumed allowing the formation of $GdVO_4$ nuclei. The deposition of nonradioactive shells is assumed to be through Ostwald ripening, where the nuclei interact with the core NCs. In this process the smallest nuclei are dissolved as a mechanism to minimize the system energy, and their matter is added to the radioactive core NCs forming a nonradioactive $GdVO_4$ shell.[47] A second shell with the same elemental composition was deposited by mixing the core + 1 shell NCs suspension with a solution containing Gd-Cit-VO_4 oligomeric species. It is expected that the volume ratio between core suspension and oligomeric species solution will influence the shell thickness.

Crystal structure

The crystal structure of the as-prepared $GdVO_4$ core and core–shell NCs is a critical parameter for the retention of radionuclides. Monazite- and zircon-type structures have demonstrated their ability to retain radionuclides, mainly actinides, for nuclear waste management.[37,48,49] The importance of these two structures relies on the low probability of transformation into an amorphous or metamict state as a result of the radiation damage caused particularly by α-decay.[37,49] The as-prepared $GdVO_4$ core and core–shell NCs have a tetragonal crystal system (zircon-type) with space group $I4_1/amd$ corresponding to $GdVO_4$ (pdf: 00-017-

026). The analysis of the crystal structure was performed using the HighScore Plus software and the International Centre for Diffraction Data database. The diffraction patterns of $GdVO_4$-Ac and $GdVO_4$-Th core and core + 2 shells NCs are shown in Fig. 1 (a) and (b), respectively. All diffraction patterns are characterized by broad Bragg reflections caused by the small size of the NCs (Fig. 1). The crystallite size was calculated using the Scherrer equation ($D = K\lambda/\beta \cos\theta$), where D is the crystallite size, λ is the wavelength of the Cu-K_α radiation, β is the full-width at half maximum of the selected reflection, θ is the Bragg angle, and K is a shape factor set as 0.9.[50] The most intense reflection corresponding to the peak located at 25°, (200) plane in the tetragonal structure, was used to calculate the crystallite size. $GdVO_4$-Th core and core + 2 shells NCs have a larger crystallite size compared to that of $GdVO_4$-Ac NCs (Table I). The difference in crystallite size between core NCs is a consequence of volume ratio of chemicals used during synthesis since parameters such as heating time and temperature were kept constant. Larger $GdVO_4$-Th core NCs were expected because of the decrease in the concentration of sodium citrate and its role as a complexing agent.[46] Additionally, the increase of sodium orthovanadate concentration results in a lower fraction of surface Gd^{3+} ions available for complexation with citrate groups, which may compromise the stability of the NCs resulting in larger growth, aggregation, or both.[46] The difference between the crystallite size of core and core + 2 shells NCs was 0.7 nm for $GdVO_4$-Ac and 2.0 nm for $GdVO_4$-Th (Table I). The larger crystallite size increase observed for $GdVO_4$-Th NCs was related to the concentration of the chemicals as discussed above and to the higher volume ratio (1:2) between the core NCs suspension and the oligomeric species solution used during shell deposition.

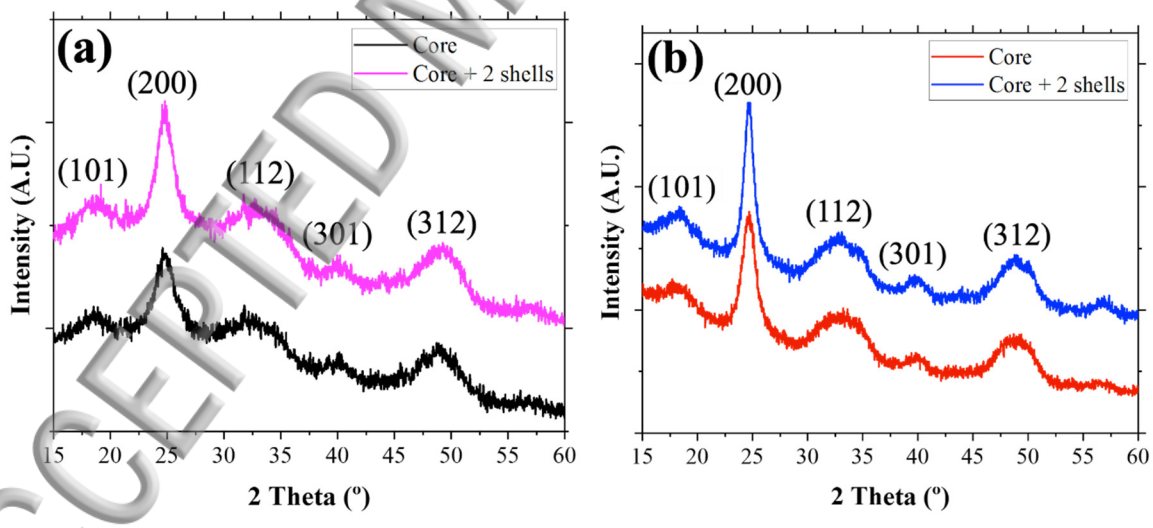

Fig. 1 Diffraction patterns of (a) $GdVO_4$-Ac and (b) $GdVO_4$-Th core and core + 2 shells NCs.

Table I Crystallite size measured for $GdVO_4$-Ac and $GdVO_4$-Th core and core + 2 shells NCs

Sample	Crystallite size (nm)	
	$Gd(^{225}Ac)VO_4$	$Gd(^{227}Th)VO_4$
Core	4.0	5.5
Core + 2 shells	4.7	7.5

Morphology and size distribution

Hydrodynamic size of $GdVO_4$ core and core + 2 shells NCs was characterized using both intensity and number distributions. The intensity distribution is related to the intensity of light scattered by particles of different sizes. Consequently, it is expected to highlight the contribution of larger particles based on Mie theory, whereas the number distribution provides a representation of the number of particles based on their size. The intensity and number distributions of $GdVO_4$ core–shell NCs are shown in Fig. 2 and Fig. S.1, respectively. The polydispersity index, mean hydrodynamic size, and standard deviation obtained from each distribution are summarized in Tables S.I and S.II. $GdVO_4$-Ac core and core + 2 shells NCs are characterized by narrow intensity [Fig. 2(a)] and number [Fig. S.1(a)] distributions, which are suitable for *in vivo* biomedical applications.[51] As shown in Fig. 2(b) and Fig. S.1(b), only the $GdVO_4$-Th core NCs are represented by narrow intensity and number distributions. The broadening observed in both distributions for $GdVO_4$-Th core + 2 shells NCs may be a consequence of particle aggregation caused by the lower concentration of sodium citrate and a lower fraction of surface Gd^{3+} ions available for complexation.[46] The particle size distribution of both as-prepared NCs is within the particle size window, 5.5–200 nm, recommended to prevent renal clearance and to avoid uptake by the reticuloendothelial system.[52] As shown in Fig. S.1(a), the number particle size distribution of $GdVO_4$-Ac core + 2 shells NCs reveals that either new NCs were created, or some of them were not covered with $GdVO_4$ shells. This could be a consequence of a combined effect between the mechanism of shell growth, Ostwald ripening, the volume ratio of chemicals, and the lack of oligomeric species added during the synthesis. The development of NCs without dense lattice shells could result in a higher fraction of radionuclides leaking from the NCs. Overall, the mean hydrodynamic size obtained from the number distribution provides a more accurate representation of the NC size compared to the intensity values, where aggregation may skew the results (Tables S.I and S.II). The presence of complexing agents such as citrate ions or counter ions from unreacted species may also contribute to an overestimation of the NCs size based on the number distribution.

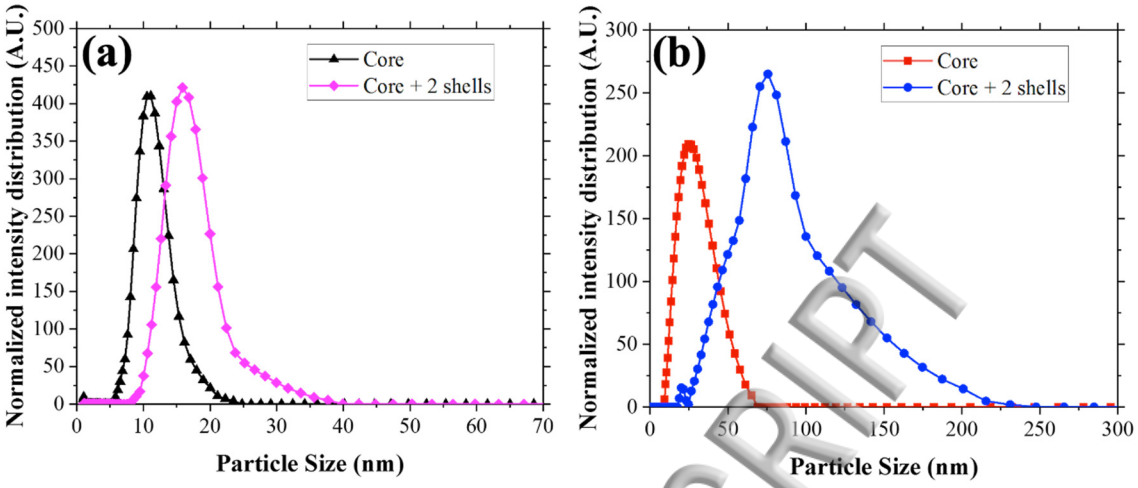

Fig. 2 Normalized intensity distributions of (a) $GdVO_4$-Ac and (b) $GdVO_4$-Th core and core + 2 shells NCs.

Transmission electron micrographs of $GdVO_4$-Ac core and core + 2 shells are characterized by aggregates of NCs having spherical and ellipsoidal shape (Figs. 3 and S.2). The insets shown in Fig. 3 reveal the existence of well-defined lattice fringes which correspond to the (200) plane in the tetragonal structure of $GdVO_4$. Individual $GdVO_4$-Ac core and core + 2 shell NCs can be identified thanks to the lattice fringes shown in the high-resolution images (Fig. S.2). A mean particle size of 3.6 ± 0.9 nm and 4.4 ± 1.0 nm was obtained for $GdVO_4$-Ac core and core + 2 shells NCs, respectively. The mean particle size for both core and core + 2 shells is consistent with their crystallite size, suggesting that the as-prepared NCs correspond to single crystals. It is expected that $GdVO_4$-Th core and core + 2 shells NCs will have spherical and ellipsoidal shape and a larger mean particle size as well as a higher tendency to aggregate compared to $GdVO_4$-Ac NCs based on the dynamic light scattering results.

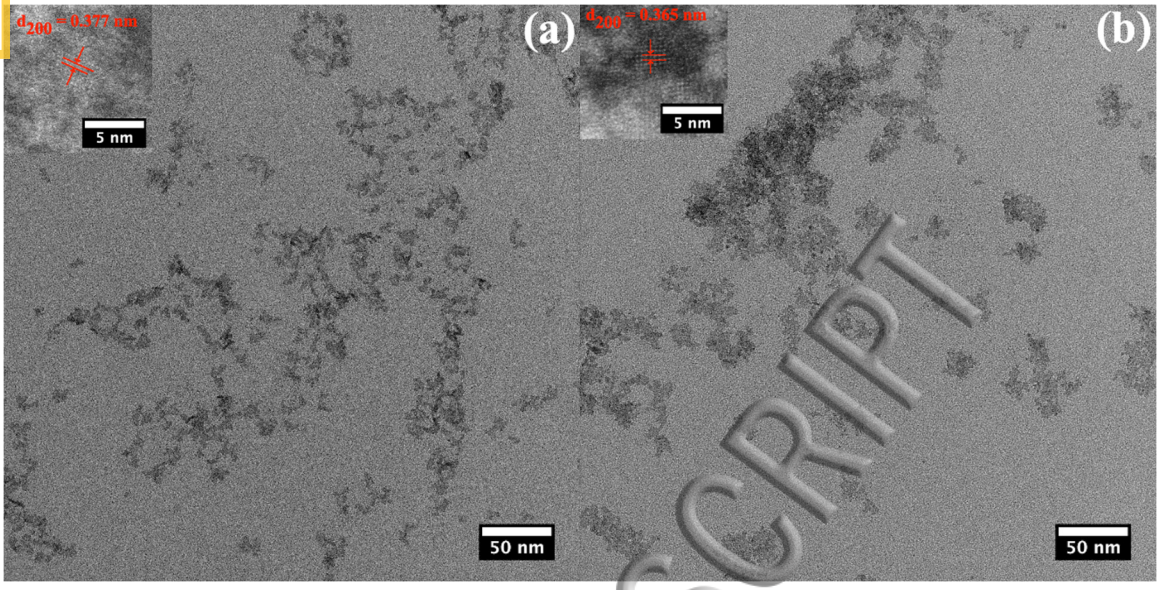

Fig. 3 Transmission electron micrographs of $GdVO_4$-Ac (a) core and (b) core + 2 shells NCs. Inserts correspond to high resolution images showing the lattice fringes of $GdVO_4$ NCs.

Zeta potential

The surface charge of as-prepared $GdVO_4$-Ac and $GdVO_4$-Th core and core + 2 shells NCs is among different parameters that may influence their biodistribution and physical stability. In Table II, the mean ζ-potential and standard deviation of as-prepared $GdVO_4$-Ac and $GdVO_4$-Th core and core + 2 shells NCs are summarized. The negative magnitude of the ζ-potential obtained is consistent with the presence of citrate groups complexed to Gd cations on the sample surface.[47] The difference between $GdVO_4$-Ac core and core + 2 shells is assumed to be related to an increase in the chemical yield and hence the number of NCs formed. In previous experiments, the magnitude of the ζ-potential has shown a decrease when the NCs concentration is lower. On the other hand, the increase in magnitude of ζ-potential between core and core + 2 shells is related to a reduction of the citrate groups that are consumed during synthesis resulting in aggregation of NCs as observed from the size distribution results (Fig. 2).

Table II ζ-potential of $GdVO_4$-Ac and $GdVO_4$-Th core and core + 2 shells NCs

Sample	**ζ-potential (mV)**	
	$Gd(^{225}Ac)VO_4$	$Gd(^{227}Th)VO_4$
Core	-17.8 ± 1.6	-33.8 ± 3.8
Core + 2 shells	-30.0 ± 2.5	-30.2 ± 1.4

Chemical yield

Chemical yield is an essential parameter to assess the fraction of radioactivity lost during synthesis, and it also provides information to evaluate the proton relaxivities of MRI contrast agents. Evaluation of chemical yield was done based on the input concentration of Gd cations used for the synthesis in $GdVO_4$ core NCs. The Gd concentration in solution was determined by ICP-OES. The as-prepared core NCs suspensions were transferred into the regenerated cellulose

membrane and dialyzed against DI water for 20 hours. Both dialyzed NCs suspension and dialysate were analyzed using ICP-OES to determine the Gd concentration. Volumetric flasks previously cleaned with 10% nitric acid were used for the preparation of ICP samples and standards. Standard preparation consisted of a 1000 ppm Gd ICP standard, obtained from Inorganic Ventures™, which was serially diluted from 100 to 0.01 ppm to construct a calibration curve. The calculated chemical yield for $GdVO_4$-Ac and $GdVO_4$-Th core NCs was 65.9 ± 2.1% and 81.9 ± 2.3%, respectively. The increase of chemical yield was caused by the modified concentration of sodium citrate and sodium orthovanadate used during synthesis. A decrease of sodium citrate concentration may promote formation and aggregation of NCs because of its role as a complexing agent, whereas the role of sodium orthovanadate in the chemical yield is related to the stoichiometry between $[VO_4]^{3-}$ and Gd^{3+} ions. Therefore, using a higher concentration of $[VO_4]^{3-}$ precursor may promote the formation of $GdVO_4$ nuclei and hence contribute to the growth of NCs. It is important to highlight that a higher concentration of Na_3VO_4 may result in a chemical yield closer to 100%, however, the complexation of citrate groups with surface Gd^{3+} ions requires the implementation of a vanadate substoichiometry (a molar ratio of vanadate/gadolinium below 1) to ensure NCs stability.[46]

MRI and relaxation time studies

The response of $GdVO_4$-Ac core NCs as positive (T_1) MRI contrast agent was tested using a suspension that was dialyzed overnight to remove unreacted species, particularly Gd^{3+} ions. The respective T_1-weigthed images obtained on the 7T BioSpec 70/30 small animal MRI scanner from $GdVO_4$-Ac core NCs at various concentrations are shown in Fig. 4(a). The increase in concentration of NCs resulted in an enhancement of the signal intensity, observed as brighter images, characteristic of positive (T_1) MRI contrast agents. Figure 4(b) shows the relationship between the concentration of Gd^{3+} ions and T_1^{-1} relaxation rates. The T_1^{-1} relaxation rate of water protons increased with higher concentration of Gd^{3+} ions [Fig. 4(b)].

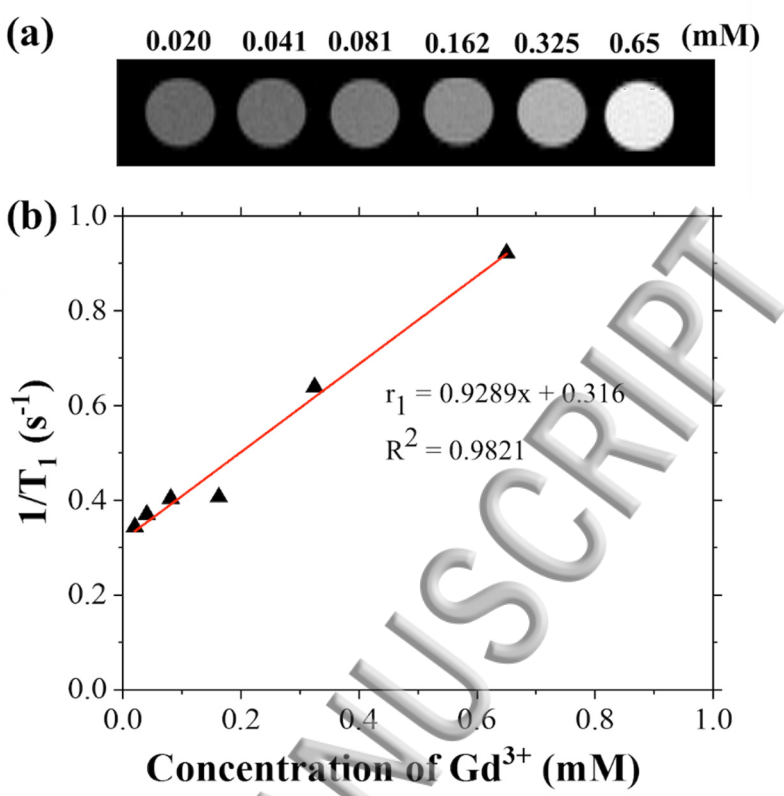

Fig. 4 (a) T_1-weighted images of various concentrations of $GdVO_4$-Ac core NCs (DI water was used as a reference). (b) Longitudinal proton relaxivity (r_1) measured for $GdVO_4$-Ac core NCs at 7T.

The calculated longitudinal proton relaxivity (r_1) has a magnitude of 0.9289 s^{-1} mM^{-1}, which suggests the potential application of $GdVO_4$ NCs as positive (T_1) MRI contrast agents. This value is comparable to the longitudinal relaxivity reported for surface functionalized $Gd_{0.9}Eu_{0.1}VO_4$ NCs, r_1 = 0.776 s^{-1} mM^{-1}.[9] However, Abdesselem *et al.* reported a longitudinal relaxivity for $GdVO_4$ NPs synthesized using the same procedure that is ~5 times higher than that obtained for $GdVO_4$-Ac core NCs.[11] This difference could be related to an increase in particle size after dialysis, attributed to NCs aggregation, since a significant broadening of the normalized intensity distribution was observed [Fig. S.3(a)]. A reduction of the concentration of citrate groups and counterions during dialysis may be the main cause behind NC aggregation based on the decrease of the mean particle size from the normalized number distribution [Fig. S.3(b)]. Overall, an increase in particle size,[4] aggregation of NCs,[53] or a combination of both may cause a decrease of the longitudinal (r_1) proton relaxivity due to a lower concentration of surface Gd^{3+} ions. Therefore, $GdVO_4$-Th core and both core + 2 shells NCs suspension are expected to have lower longitudinal (r_1) proton relaxivities because of their large particle size, tendency to aggregate, or a combination of both.

***In vitro* Retention of ^{225}Ac, ^{227}Th, and Decay Daughters**

$GdVO_4$ core and core + 2 shells NCs were evaluated as alternatives for the retention of ^{225}Ac, ^{221}Fr, ^{227}Th, and ^{223}Ra while providing functionalities for molecular imaging. *In*

vitro retention testing was performed using a setup consisting in the dialysis of the radioactive NCs suspensions against DI water and the quantification of the activity associated with each radionuclide from dialysate aliquots taken periodically and assayed in a HPGe. The error bars displayed in Figs. 5 and 6 were calculated by propagation of error considering the uncertainties from pipetting, detector efficiency, and γ-ray characterization. Figure 5(a) shows the leakage of ^{225}Ac from Gd(^{225}Ac)VO_4 and Gd(^{225}Ac)VO_4/2$GdVO_4$ NCs. The leakage of ^{225}Ac from the core NCs reached a maximum ~15.0 ± 0.9%, which is related to unreacted ^{225}Ac cations that were not retained within the NCs and that remained as ^{225}Ac-Cit complexes.[54] Because the water was replaced after the first and eleventh day, the increase in activity from days 3–10 and 12–20 is related to a slow clearance of these ^{225}Ac-Cit complexes during dialysis. The deposition of two nonradioactive $GdVO_4$ shells significantly improves the retention of ^{225}Ac cations, where the activity seems to increase over time to a maximum of 2.4 ± 0.2% [Fig. 5(a)]. The overall enhancement in the retention of ^{225}Ac within Gd(^{225}Ac)VO_4/2$GdVO_4$ is related to the consumption of the ^{225}Ac-Cit complexes during the deposition of nonradioactive shells since no intermediate cleaning step was used. The leakage of the first decay daughter, ^{221}Fr, from core and core + 2 shells NCs over 30 days is shown in Fig. 5(b). The leakage of ^{221}Fr from Gd(^{225}Ac)VO_4 was 40.6 ± 2.4% after 2 days; however it increased to ~69.5 ± 4.9% after 23 days in dialysis. The deposition of two nonradioactive $GdVO_4$ shells improved the retention of ^{221}Fr by ~20% with respect to core NCs [Fig. 5(b)]. This enhancement is related to the presence of a dense lattice structure that acts as a physical barrier against the leakage of radionuclides.[22,23,54] The retention of ^{213}Bi was higher to that of ^{221}Fr for both Gd(^{225}Ac)VO_4 and Gd(^{225}Ac)VO_4/2$GdVO_4$ NCs (Fig. S.3). The maximum leakage for ^{213}Bi from Gd(^{225}Ac)VO_4 and Gd(^{225}Ac)VO_4/2$GdVO_4$ was 22.5 ± 1.3% and 19.6 ± 1.9%, respectively. Formation of ^{213}Bi-citrate compounds were suggested as a possible mechanism for the observed decrease in the ^{213}Bi leakage to the dialysate in comparison to ^{221}Fr.[54]

The retention of ^{221}Fr in Gd(^{225}Ac)VO_4 is comparable to the results obtained with 100 nm polymersomes, which retained ~37% of ^{221}Fr.[35] Nonetheless, the retention of both ^{225}Ac and ^{221}Fr in Gd(^{225}Ac)VO_4 NCs falls short of the results obtained for $La_{0.5}Gd_{0.5}PO_4$ core NPs, which retained ~99% of ^{225}Ac and ~60% of ^{221}Fr after 3 weeks.[22] For Gd(^{225}Ac)VO_4/2$GdVO_4$ NCs, the retention of both ^{225}Ac and ^{221}Fr was closer to the one reported for $La_{0.5}Gd_{0.5}PO_4$ core + 2 shells NPs (99.4% for ^{225}Ac and ~69% for ^{221}Fr).[22] It is expected that the leakage probability of decay daughters will increase because of the ^{225}Ac atoms that were retained within the nonradioactive $GdVO_4$ shells. A simple experiment where the radioactive core suspension was dialyzed before the deposition of shells showed that the leakage of ^{221}Fr reached a maximum ~32% after 2 weeks, which is comparable to the results obtained with $La_{0.5}Gd_{0.5}PO_4$ core + 2 shells NPs.[22] These experiments have shown that ^{221}Fr cations are not quantitatively retained in Gd(^{225}Ac)VO_4 and Gd(^{225}Ac)VO_4/2$GdVO_4$ NCs; consequently, toxicity to normal organs, particularly the kidney, could be expected during *in vivo* applications.[55] Variation of synthesis parameters to

deposit thicker $GdVO_4$ shells and intermediate cleaning procedures are expected to enhance the retention of decay daughters.

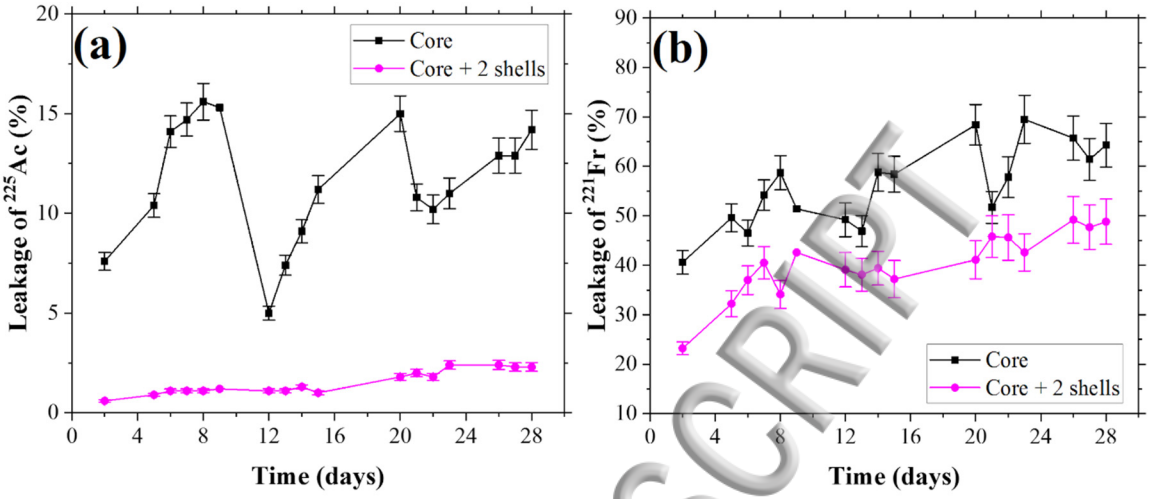

Fig. 5 Leakage of (a) ^{225}Ac and (b) ^{221}Fr from Gd(^{225}Ac)VO_4 and Gd(^{225}Ac)VO_4/2$GdVO_4$ NCs.

In vitro retention of ^{227}Th and its first decay daughter, ^{223}Ra, was assessed in Gd(^{227}Th)VO_4 and Gd(^{227}Th)VO_4/2$GdVO_4$ NCs. Particular interest has been placed in these two α-emitting radionuclides based on their long half-life and the ability to produce them in clinically relevant quantities.[43] Xofigo®, ^{223}Ra dichloride (Bayer HealthCare Pharmaceuticals Inc.), was approved in 2013 by the U.S. Food and Drug Administration for the treatment of patients with castration-resistant prostate cancer.[56] The promising results obtained by Xofigo® have encouraged the implementation of ^{227}Th and ^{223}Ra for the treatment of disseminated diseases and tumors in soft tissue upon successful retention at the target site. Figure 6(a) shows leakage of ^{227}Th from Gd(^{227}Th)VO_4 and Gd(^{227}Th)VO_4/2$GdVO_4$. The leakage measured for the core NCs was ~3% for the first 15 days, and then it decreased to 1.6 ± 0.3% at day 18 [Fig. 6(a)]. Even though the samples were analyzed for over 30 days, the activity of ^{227}Th in the dialysate was below the detection limit of the HPGe detector. Similarly, the leakage of ^{227}Th from Gd(^{227}Th)VO_4/2$GdVO_4$ was <1.5% in the first 12 days in dialysis, with no activity detected afterward [Fig. 6(a)]. These results demonstrate that ^{227}Th cations are successfully immobilized within the tetragonal structure of $GdVO_4$ and do not easily form Th-Cit complexes in comparison to ^{225}Ac. The leakage of ^{223}Ra from core NCs was 10.0 ± 0.7% after 1 day in dialysis and then increased up to 39.0 ± 2.2% after 2 weeks. The deposition of two nonradioactive $GdVO_4$ shells resulted in a decrease of ^{223}Ra leakage to ~25% [Fig. 6(b)]. For ^{211}Pb (Fig. S.4), the maximum leakage observed was 46.6 ± 3.1% and 36.2 ± 2.5% from Gd(^{227}Th)VO_4 and Gd(^{227}Th)VO_4/2$GdVO_4$, respectively. The fact that ^{211}Pb is the fourth daughter in the decay chain of ^{227}Th is the reason for the higher leakage of ^{211}Pb with respect to ^{223}Ra. These results demonstrate the potential of $GdVO_4$ core–shell NCs as carriers of ^{227}Th for targeted alpha therapy because the retention of ~75% of ^{223}Ra activity could mitigate the myelosuppression caused by free ^{223}Ra cations observed in rodent studies using CD70 targeted ^{227}Th conjugate.[30] Furthermore, the fraction of activity released from the NCs could be within the therapeutic window where acceptable myelotoxicity is caused by ^{223}Ra.[39]

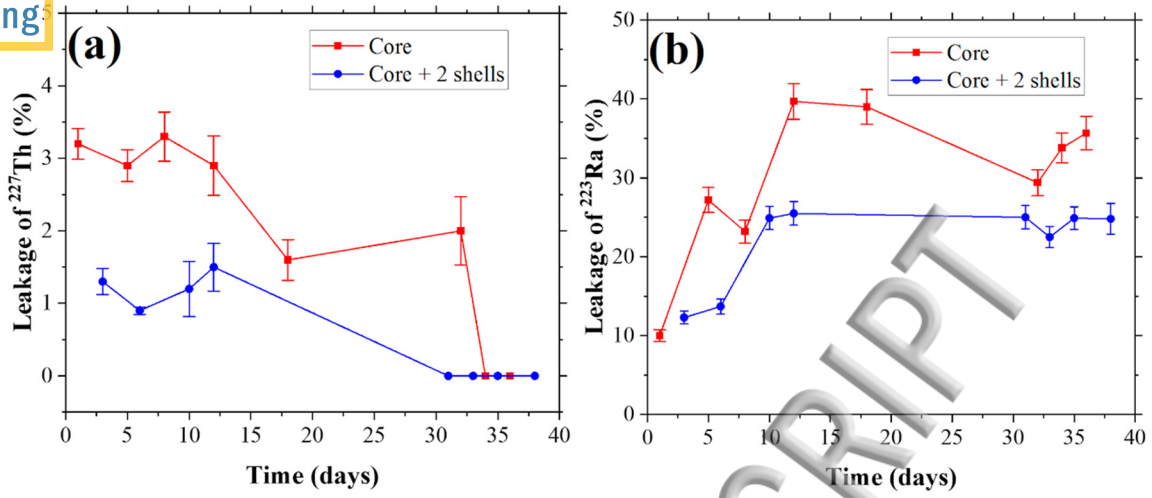

Fig. 6 Leakage of (a) ^{227}Th and (b) ^{223}Ra from Gd(^{227}Th)VO_4 and Gd(^{227}Th)VO_4/2$GdVO_4$ NCs.

Although $GdVO_4$ NCs doped with either ^{225}Ac or ^{227}Th displayed partial retention of their first decay daughters, it is expected that both ^{221}Fr and ^{223}Ra will leak completely from the NCs based on their range in $GdVO_4$. Francium-221 ions with a recoil energy of 105.5 keV (calculated from classical conservation of momentum) are expected to have a range of ~85 nm and ~26 nm in H_2O (ρ = 1 g/cm^3) and $GdVO_4$ (crystal density of ρ = 5.47 g/cm^3) based on calculations made using the Stopping and Range of Ion in Matter software.[57] Similarly, the range of ^{223}Ra (E = 108.4 keV) in H_2O and $GdVO_4$ is ~87 nm and ~27 nm, respectively. It is assumed that the partial retention of ^{221}Fr, ^{213}Bi, ^{223}Ra, and ^{211}Pb is associated with the conversion of a fraction of the recoil energy to translational energy of the NC, their implantation in adjacent NCs, and adsorption by surface groups (hydroxyl and carboxylic).[28,29,54,58,59] The fact that inorganic $GdVO_4$ core and core + 2 shells NCs are very rigid and dense suggests the possibility that a faction of the recoil energy is transferred to the translational energy of NCs.[20,54] The implantation of decay daughters in adjacent NCs is assumed based on the dynamic light scattering results (Fig. 2), where both $GdVO_4$ core and core + 2 shells NCs formed aggregates with a mean size similar to the range of decay daughters in $GdVO_4$. $GdVO_4$-Th NCs had a broader particle size distribution, which may have contributed to a higher retention of ^{223}Ra with respect to that of ^{221}Fr in $GdVO_4$-Ac (Fig. 2). In addition, the decay daughters out of the NCs are thermalized quickly (~30 nm) and may form complexes with the NC surface groups (hydroxyl and carboxylic). It is expected that ^{221}Fr, as a singly charged alkali metal ion, will have a lower probability of adsorption by hydroxyl and carboxylic groups compared to that of ^{223}Ra cations.[20]

The radiochemical yield of ^{225}Ac and ^{227}Th was calculated based on the initial activity in the NCs suspensions, the activity lost during synthesis in the conical vials and pipettes, and the total activity lost during dialysis. The latter is particularly important because a significant fraction of radionuclides could remain in solution as free cations or complexes. The radiochemical yield of ^{225}Ac after multiple synthesis (n = 3) was 77.1 ± 13.2% and 96.6 ± 1.6% for Gd(^{225}Ac)VO_4 and Gd(^{225}Ac)VO_4/2$GdVO_4$, respectively. The radiochemical yield for the core NCs is in agreement with the chemical yield calculated from ICP-OES for $GdVO_4$-Ac. The

yield of Gd(^{225}Ac)VO_4 is comparable to the value obtained for gold-coated $LnPO_4$ core–shell NPs (76%),[22] and it is higher than that of polymer vesicles[35] and ^{225}Ac-DOTA-IgG,[60] which had a loading efficiency of 67% and <10%, respectively. The radiochemical yield of ^{227}Th based on a single measurement was 62.9 ± 2.7% and 81.9 ± 1.2% for Gd(^{227}Th)VO_4 and Gd(^{227}Th)VO_4/2$GdVO_4$ NCs, respectively. Although the radiochemical yield of both core and core + 2 shells NCs is lower than that of targeted ^{227}Th conjugates (>95%),[30,39,40] the partial retention of radionuclides, the potential to increase the specific activity, and the ability to incorporate multiple functionalities, make $GdVO_4$ suitable for targeted alpha therapy and theranostic applications. Based on the chemical and radiochemical yields, we estimated that in the preparations containing 50 μCi of ^{225}Ac and 32 μCi of ^{227}Th, the atomic ratios of Ac to Gd and Th to Gd were approximately 2.2×10^{-7} and 1.1×10^{-7}, respectively. Considering that a 5-nm diameter $GdVO_4$ NC contains on the order of 1000 Gd atoms, the average number of ^{225}Ac and ^{227}Th atoms per $GdVO_4$ NCs are 2×10^{-4} and 1×10^{-4} (i.e. one ^{225}Ac atom per ~5000 $GdVO_4$ NCs, or one ^{227}Th atom per ~10000 NCs), respectively. Consequently, there is ample capacity in $GdVO_4$ NCs to accommodate an increase in either the ^{225}Ac or ^{227}Th activity from μCi to mCi levels for targeted alpha therapy and nuclear imaging.[20] For both actinides, the deposition of shells on core NCs caused a decrease in leakage of decay daughters as well as an increase in radiochemical yield with respect to core NCs. The increase in radiochemical yield may be related to the consumption of unreacted species and hence immobilization of radionuclides during the deposition of nonradioactive shells. These results demonstrate the potential application $GdVO_4$ core–shell NCs as an alternative platform for the encapsulation of α-emitting radionuclides, ^{225}Ac and ^{227}Th, for cancer treatment. The main advantages of $GdVO_4$ NCs as radionuclide carriers for targeted radionuclide therapy are related to the partial retention of α-emitting radionuclides and decay daughters, the ability to use $GdVO_4$ NCs as MRI contrast agent, and the simple and less time-consuming synthesis procedure. For instance, polymer vesicles proposed for targeted alpha therapy required large particle sizes (>100 nm) to achieve a similar retention of ^{221}Fr as the one reported in this work.[61] In addition, multiple functionalities for molecular imaging can be included to $GdVO_4$ NCs via a simple adjustment of the lanthanide concentration, whereas for polymer vesicles a fluorescence dye and/or contrast agent must be added.[62]

Conclusions

Immobilization of therapeutically relevant α-emitting radionuclides, ^{225}Ac and ^{227}Th, and *in vitro* retention of decay daughters within $GdVO_4$ core and core + 2 shells NCs was evaluated in this work. Spherical NCs with a tetragonal structure were synthesized by a precipitation route that is suitable for radiochemical synthesis. Retention of α-emitting radionuclides and decay daughters within $GdVO_4$ NCs was influenced by the parent radionuclide, number of shells, and cleaning steps followed during shell deposition. The deposition of two nonradioactive $GdVO_4$ shells enhanced the *in vitro* retention of decay daughters ^{221}Fr and ^{223}Ra by 20% and 15%, respectively. The as-prepared $GdVO_4$ core NCs have potential application as an MRI contrast

agent based on their longitudinal proton relaxivity (r_1), 0.9289 s^{-1} mM^{-1}. The suitable radiochemical synthesis, *in vitro* retention, and proton relaxivity suggest the promising use of $GdVO_4$ core–shell NCs as a multifunctional diagnostic and therapeutic platform for biomedical applications. Future experiments will assess the stability of $GdVO_4$ NCs in biological relevant solutions as well as their functionalization and bioconjugation to attach targeting moieties that will direct $GdVO_4$ NCs to the site of interest.

Supplementary material

See supplementary material for additional physical and radiochemical characterization of the $GdVO_4$ core and core + 2 shells nanomaterials

Acknowledgements

This research was supported by (i) Virginia Commonwealth University with the support of the Mechanical and Nuclear Engineering Department and the NRC-HQ-84-14-FOA-002, Faculty Development Program in Radiation Detection and Health Physics at Virginia Commonwealth University, (ii) the U.S. Department of Energy Isotope Program within the Office of Nuclear Physics, and (iii) an appointment to the Oak Ridge National Laboratory Nuclear Engineering Science Laboratory Synthesis program, sponsored by the U.S. Department of Energy and administered by the Oak Ridge Institute for Science and Education. We would like to thank the staff of the Nuclear and Radiochemistry Group at Oak Ridge National Laboratory, the staff at the Nanomaterials Core Characterization Facility from the College of Engineering, and the Instrumentation Laboratory from the Department of Chemistry at Virginia Commonwealth University. The authors are thankful to Dr. Qiu Zhang and Dr. David Cullen from Oak Ridge National Laboratory for their assistance.

Conflicts of Interest

There are no conflicts to declare.

References

[1] Y. Zhang, W. Wei, G.K. Das, and T.T. Yang Tan, Journal of Photochemistry and Photobiology C: Photochemistry Reviews **20**, 71 (2014).

[2] R.D. Teo, J. Termini, and H.B. Gray, Journal of Medicinal Chemistry **59**, 6012 (2016).

[3] H. Wen and F. Wang, *Lanthanide-Doped Nanoparticles*, Second Edi (Elsevier Ltd, 2014).

[4] H. Dong, S.-R. Du, X.-Y. Zheng, G.-M. Lyu, L.-D. Sun, L.-D. Li, P.-Z. Zhang, C. Zhang, and C.-H. Yan, Chemical Reviews **115**, 10725 (2015).

[5] C. Bouzigues, T. Gacoin, and A. Alexandrou, ACS Nano **5**, 8488 (2011).

[6] T.J. Fraum, D.R. Ludwig, M.R. Bashir, and K.J. Fowler, Journal of Magnetic Resonance Imaging **46**, 338 (2017).

[7] A. Escudero, A.I. Becerro, C. Carrillo-Carrión, N.O. Núñez, M. V. Zyuzin, M. Laguna, D. González-Mancebo, M. Ocaña, and W.J. Parak, Nanophotonics **0**, 1568 (2017).

[8] Y. Wu, Y. Sun, X. Zhu, Q. Liu, T. Cao, J. Peng, Y. Yang, W. Feng, and F. Li, Biomaterials **35**, 4699 (2014).

[9] N.O. Nuñez, S. Rivera, D. Alcantara, J.M. de la Fuente, J. García-Sevillano, and M. Ocaña, Dalton Transactions **42**, 10725 (2013).

[10] T. Kim, N. Lee, Y. Il Park, J. Kim, J. Kim, E.Y. Lee, M. Yi, B.-G. Kim, T. Hyeon, T. Yu, and H. Bin Na, RSC Adv. **4**, 45687 (2014).

[11] M. Abdesselem, M. Schoeffel, I. Maurin, R. Ramodiharilafy, G. Autret, O. Clément, P.L. Tharaux, J.P. Boilot, T. Gacoin, C. Bouzigues, and A. Alexandrou, ACS Nano **8**, 11126 (2014).

[12] V. Muhr, M. Buchner, T. Hirsch, D.J. Jovanovi, S.D. Doli, M.D. Dramianin, and O.S. Wolfbeis, Sensors and Actuators, B: Chemical **241**, 349 (2017).

[13] N. Shanta Singh, R.S. Ningthoujam, G. Phaomei, S.D. Singh, A. Vinu, and R.K. Vatsa, Dalton Transactions (Cambridge, England : 2003) **41**, 4404 (2012).

[14] D.J. Jovanović, A. Chiappini, L. Zur, T. V. Gavrilović, T.N. Lam Tran, A. Chiasera, A. Lukowiak, K. Smits, M.D. Dramićanin, and M. Ferrari, Optical Materials **76**, 308 (2018).

[15] T. V. Gavrilović, D.J. Jovanović, V. Lojpur, and M.D. Dramićanin, Sci. Rep. **4**, 4209 (2014).

[16] J.H. Oh, B.K. Moon, B.C. Choi, J.H. Jeong, J.H. Kim, and H.S. Lee, Solid State Sciences **42**, 1 (2015).

[17] T. V. Gavrilovic, D.J. Jovanovc, K. Smits, and M.D. Dramicanin, Dyes and Pigments **126**, 1 (2016).

[18] Y. Liang, H.M. Noh, J. Xue, H. Choi, S.H. Park, B.C. Choi, J.H. Kim, and J.H. Jeong, Materials and Design **130**, 190 (2017).

[19] C.-Y. Chou, M. Abdesselem, C. Bouzigues, M. Chu, A. Guiga, T.-H. Huang, F. Ferrage, T. Gacoin, A. Alexandrou, and D. Sakellariou, Scientific Reports **7**, 44770 (2017).

[20] J. Woodward, S.J. Kennel, A. Stuckey, D. Osborne, J. Wall, A.J. Rondinone, R.F. Standaert, and S. Mirzadeh, Bioconjugate Chemistry **22**, 766 (2011).

[21] M.F. McLaughlin, J. Woodward, R.A. Boll, J.S. Wall, A.J. Rondinone, S.J. Kennel, S. Mirzadeh, and J.D. Robertson, PLoS ONE **8**, 2 (2013).

[22] B.M.F. McLaughlin, J. Woodward, R.A. Boll, A.J. Rondinone, S. Mirzadeh, and J.D. Robertson, Radiochim **101**, 595 (2013).

[23] J.V. Rojas, J.D. Woodward, N. Chen, A.J. Rondinone, C.H. Castano, and S. Mirzadeh, Nuclear Medicine and Biology **42**, 614 (2015).

[24] M.F. McLaughlin, D. Robertson, P.H. Pevsner, J.S. Wall, S. Mirzadeh, and S.J. Kennel, Cancer Biotherapy & Radiopharmaceuticals **29**, 34 (2014).

[25] N. Sobol, L. Sutherlin, E. Cedrowska, J. Schorp, C. Rodríguez-Rodríguez, J. Lattimer, D.C. Miller, P. Pevsner, and J.D. Robertson, APL Bioengineering **2**, 016101 (2018).

[26] B.I. Kharisov, O. V Kharissova, and S.S. Berdonosov, Recent Patents on Nanotechnology **8**, 79 (2014).

[27] M. Toro-González, D.M. Clifford, R. Copping, S. Mirzadeh, and J.V. Rojas, J Nanopart Res **20**, 238 (2018).

[28] R.M. de Kruijff, H.T. Wolterbeek, and A.G. Denkova, Pharmaceuticals **8**, 321 (2015).

[29] E. Cędrowska, M. Pruszynski, A. Majkowska-Pilip, S. Męczyńska-Wielgosz, F. Bruchertseifer, A. Morgenstern, and A. Bilewicz, Journal of Nanoparticle Research **20**, 83 (2018).

[30] U.B. Hagemann, D. Mihaylova, S.R. Uran, J. Borrebaek, D. Grant, R.M. Bjerke, J. Karlsson, and A.S. Cuthbertson, Oncotarget **8**, 56311 (2017).

[31] A. Piotrowska, S. Męczyńska-Wielgosz, A. Majkowska-Pilip, P. Koźmiński, G. Wójciuk, E. Cędrowska, F. Bruchertseifer, A. Morgenstern, M. Kruszewski, and A. Bilewicz, Nuclear Medicine and Biology **47**, 10 (2017).

[32] A. Piotrowska, E. Leszczuk, F. Bruchertseifer, A. Morgenstern, and A. Bilewicz, Journal of Nanoparticle Research **15**, 1 (2013).

[33] S. Sofou, International Journal of Nanomedicine **3**, 181 (2008).

[34] H. Song, R.F. Hobbs, R. Vajravelu, D.L. Huso, C. Esaias, C. Apostolidis, A. Morgenstern, and G. Sgouros, Cancer Research **69**, 8941 (2009).

[35] G. Wang, R.M. De Kruijff, A. Rol, L. Thijssen, E. Mendes, A. Morgenstern, F. Bruchertseifer, M.C.A. Stuart, H.T. Wolterbeek, A.G. Denkova, R.M. de Kriujff, A. Rol, L. Thijssen, E. Mendes, A. Morgenstern, F. Bruchertseifer, M.C.A. Stuart, H.T. Wolterbeek, and A.G. Denkova, Applied Radiation and Isotopes **85**, 45 (2014).

[36] R.H. Larsen, J. Borrebaek, J. Dahle, K.B. Melhus, C. Krogh, M.H. Valan, and Ø.S. Bruland, Cancer Biotherapy & Radiopharmaceuticals **22**, 431 (2007).

[37] a E. Grechanovsky, N.N. Eremin, and V.S. Urusov, Lattice Dynamics **55**, 1929 (2013).

[38] J. Dahle, J. Borrebaek, T.J. Jonasdottir, A.K. Hjelmerud, K.B. Melhus, Ø.S. Bruland, O.W. Press, and R.H. Larsen, Blood **110**, 2049 (2007).

[39] J. Dahle, J. Borrebæk, K.B. Melhus, Ø.S. Bruland, G. Salberg, D.R. Olsen, and R.H. Larsen, Nuclear Medicine and Biology **33**, 271 (2006).

[40] U.B. Hagemann, K. Wickstroem, E. Wang, A.O. Shea, K. Sponheim, J. Karlsson, R.M. Bjerke, O.B. Ryan, and A.S. Cuthbertson, Molecular Cancer Therapeutics **15**, 2422 (2016).

[41] J. Dahle, Ø.S. Bruland, and R.H. Larsen, International Journal of Radiation Oncology Biology Physics **72**, 186 (2008).

[42] J. Dahle, C. Krogh, K.B. Melhus, J. Borrebæk, R.H. Larsen, and Y. Kvinnsland, International Journal of Radiation Oncology Biology Physics **75**, 886 (2009).

[43] J. Dahle and R. Larsen, Current Radiopharmaceuticalse **1**, 209 (2008).

[44] Y.S. Kim and M.W. Brechbiel, Tumor Biology **33**, 573 (2012).

[45] R.A. Boll, D. Malkemus, and S. Mirzadeh, Applied Radiation and Isotopes **62**, 667 (2005).

[46] A. Huignard, V. Buissette, G. Laurent, T. Gacoin, and J.P. Boilot, Chemistry of Materials **14**, 2264 (2002).

[47] P.W. Voorhees, Journal of Statistical Physics **38**, 231 (1985).

[48] a. Meldrum, L. Boatner, and R. Ewing, Physical Review B **56**, 13805 (1997).

[49] F. Goubard, P. Griesmar, and A. Tabuteau, Journal of Solid State Chemistry **178**, 1898 (2005).

[50] U. Holzwarth and N. Gibson, Nature Nanotechnology **6**, 534 (2011).

[51] Z. Gu, L. Yan, G. Tian, S. Li, Z. Chai, and Y. Zhao, Advanced Materials **25**, 3758 (2013).

[52] L. Zhang, H. Chen, L. Wang, T. Liu, J. Yeh, G. Lu, L. Yang, and H. Mao, Nanotechnology, Science and Applications **3**, 159 (2010).

[53] Q.L. Vuong, S. Van Doorslaer, J.L. Bridot, C. Argante, G. Alejandro, R. Hermann, S. Disch, C. Mattea, S. Stapf, and Y. Gossuin, Magnetic Resonance Materials in Physics, Biology and Medicine **25**, 467 (2012).

[54] M. Toro-González, R. Copping, S. Mirzadeh, and J.V. Rojas, J. Mater. Chem. B **6**, 7985 (2018).

[55] S.J. Kennel, L.L. Chappell, K. Dadachova, M.W. Brechbiel, T.K. Lankford, I. a Davis, M. Stabin, and S. Mirzadeh, Cancer Biotherapy & Radiopharmaceuticals **15**, 235 (2000).

[56] P.G. Kluetz, W. Pierce, V.E. Maher, H. Zhang, S. Tang, P. Song, Q. Liu, M.T. Haber, E.E. Leutzinger, A. Al-Hakim, W. Chen, T. Palmby, E. Alebachew, R. Sridhara, A. Ibrahim, R. Justice, and R. Pazdur, Clinical Cancer Research **20**, 9 (2014).

[57] J.F. Ziegler, M.D. Ziegler, and J.P. Biersack, *SRIM-The Stopping and Range of Ions in Matter (2010)* (2010).

[58] J. Kozempel and M. Vlk, Recent Patents on Nanomedicine **4**, 71 (2015).

[59] U. Holzwarth, I.O. Jimenez, and L. Calzolai, EJNMMI Radiopharmacy and Chemistry **3**, 9 (2018).

[60] S. Sofou, B.J. Kappel, J.S. Jaggi, M.R. Mcdevitt, D.A. Scheinberg, and G. Sgouros, Bioconjugate Chemistry **18**, 2061 (2007).

[61] R.M. De Kruijff, K. Drost, L. Thijssen, A. Morgenstern, F. Bruchertseifer, D. Lathouwers, H.T. Wolterbeek, and A.G. Denkova, Applied Radiation and Isotopes **128**, 183 (2017).

[62] R.M. de Kruijff, A.J.G.M. van der Meer, C.A.A. Windmeijer, J.J.M. Kouwenberg, A. Morgenstern, F. Bruchertseifer, P. Sminia, and A.G. Denkova, European Journal of Pharmaceutics and Biopharmaceutics **127**, 85 (2018).

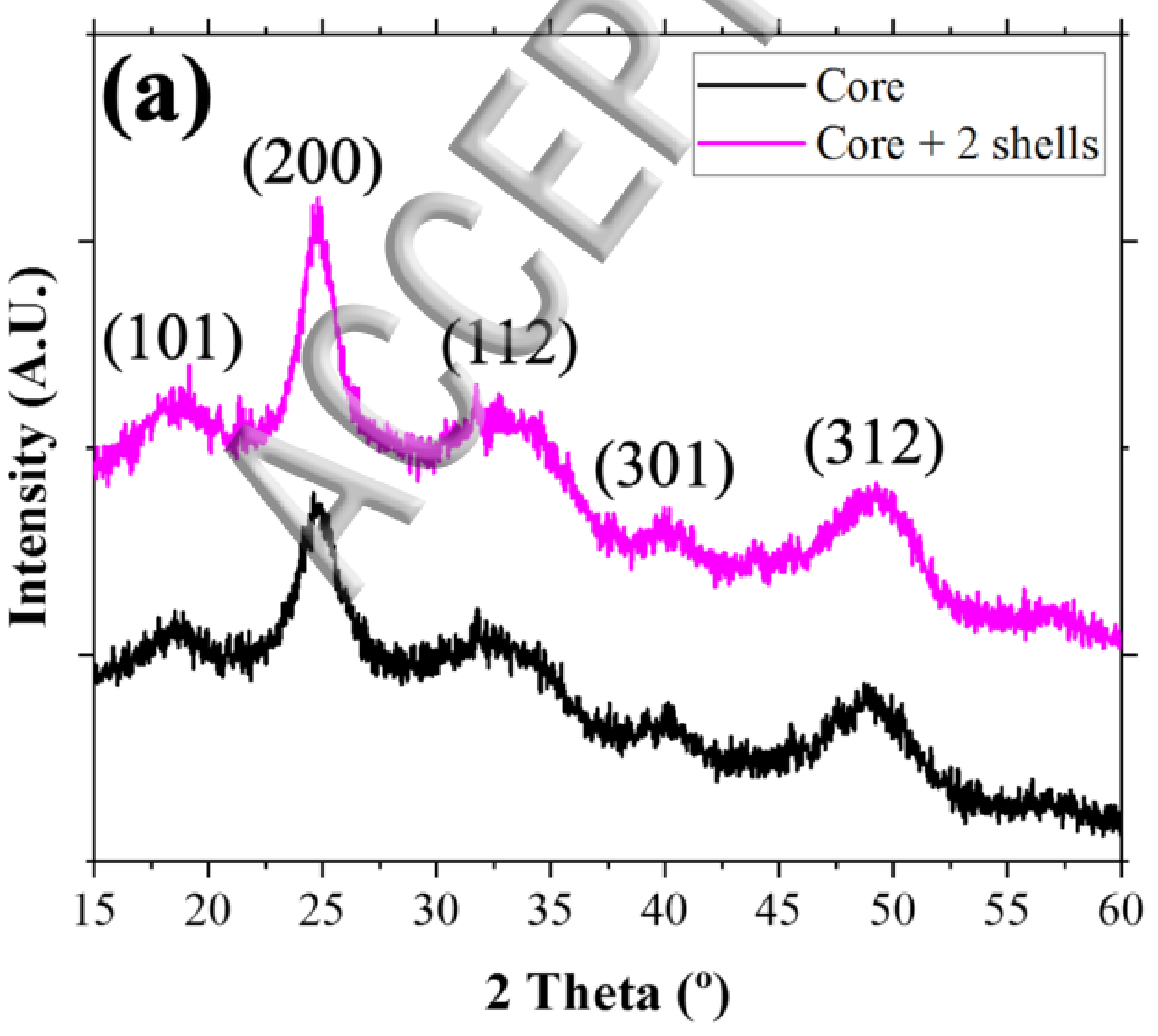
(a)
Core
Core + 2 shells
(200)
(101)
(112)
(301)
(312)
Intensity (A.U.)
15
20
25
30
35
40
45
50
55
60
2 Theta (°)

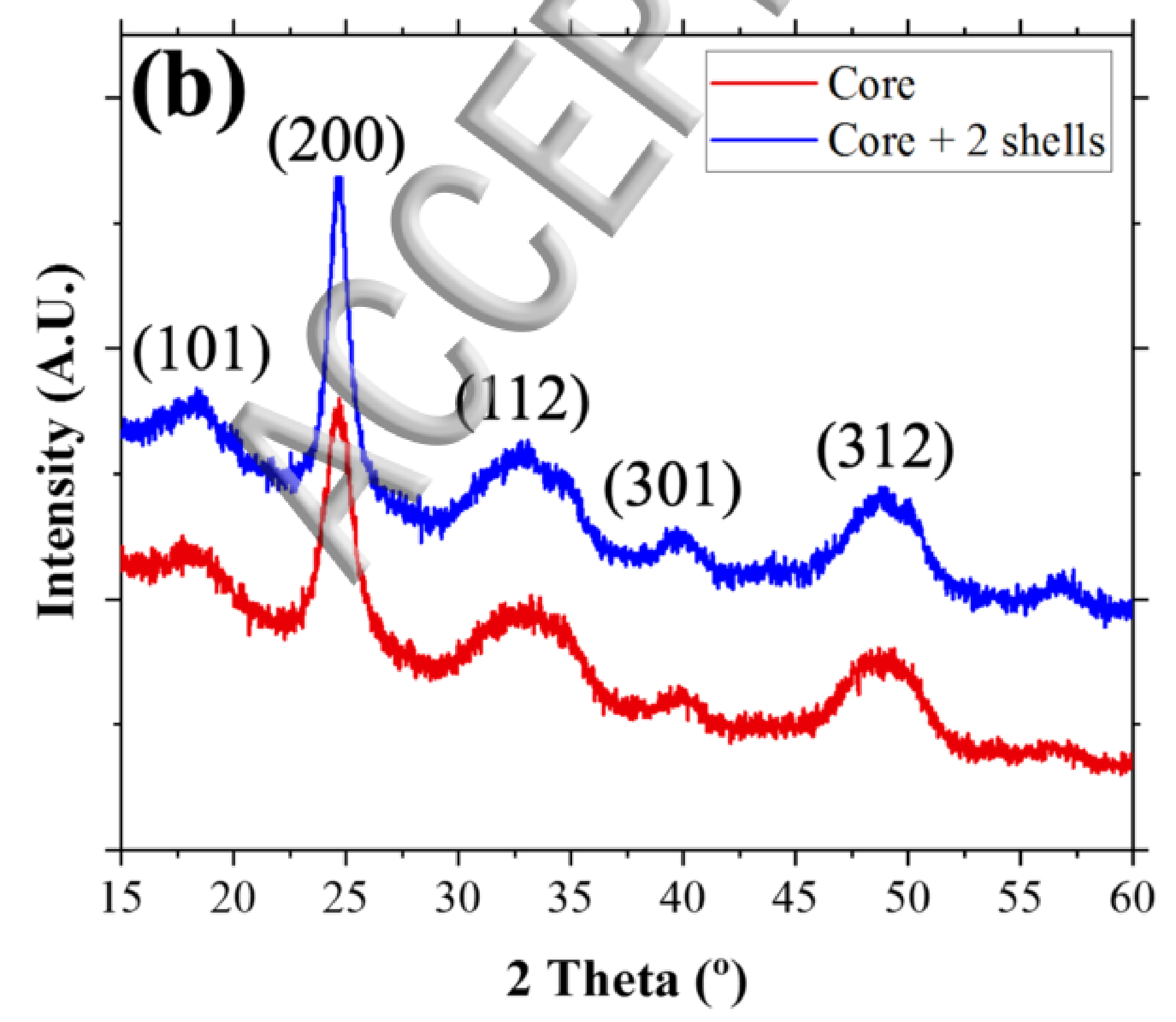
(b)
Core
Core + 2 shells
(200)
(101)
(112)
(301)
(312)
Intensity (A.U.)
15
20
25
30
35
40
45
50
55
60
2 Theta (°)

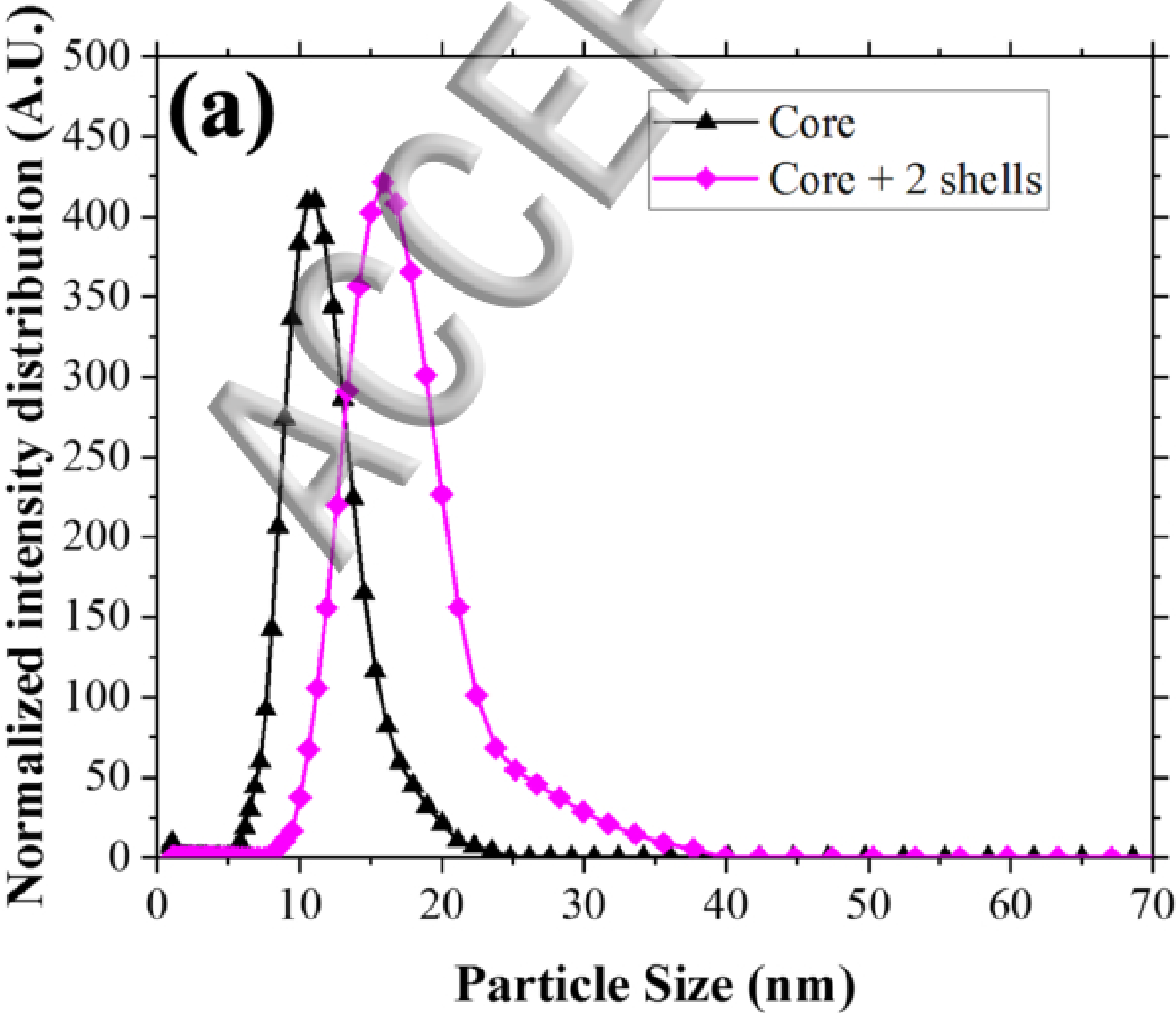
(a)
Core
Core + 2 shells
Normalized intensity distribution (A.U.)
Particle Size (nm)
0
50
100
150
200
250
300
350
400
450
500
0
10
20
30
40
50
60
70

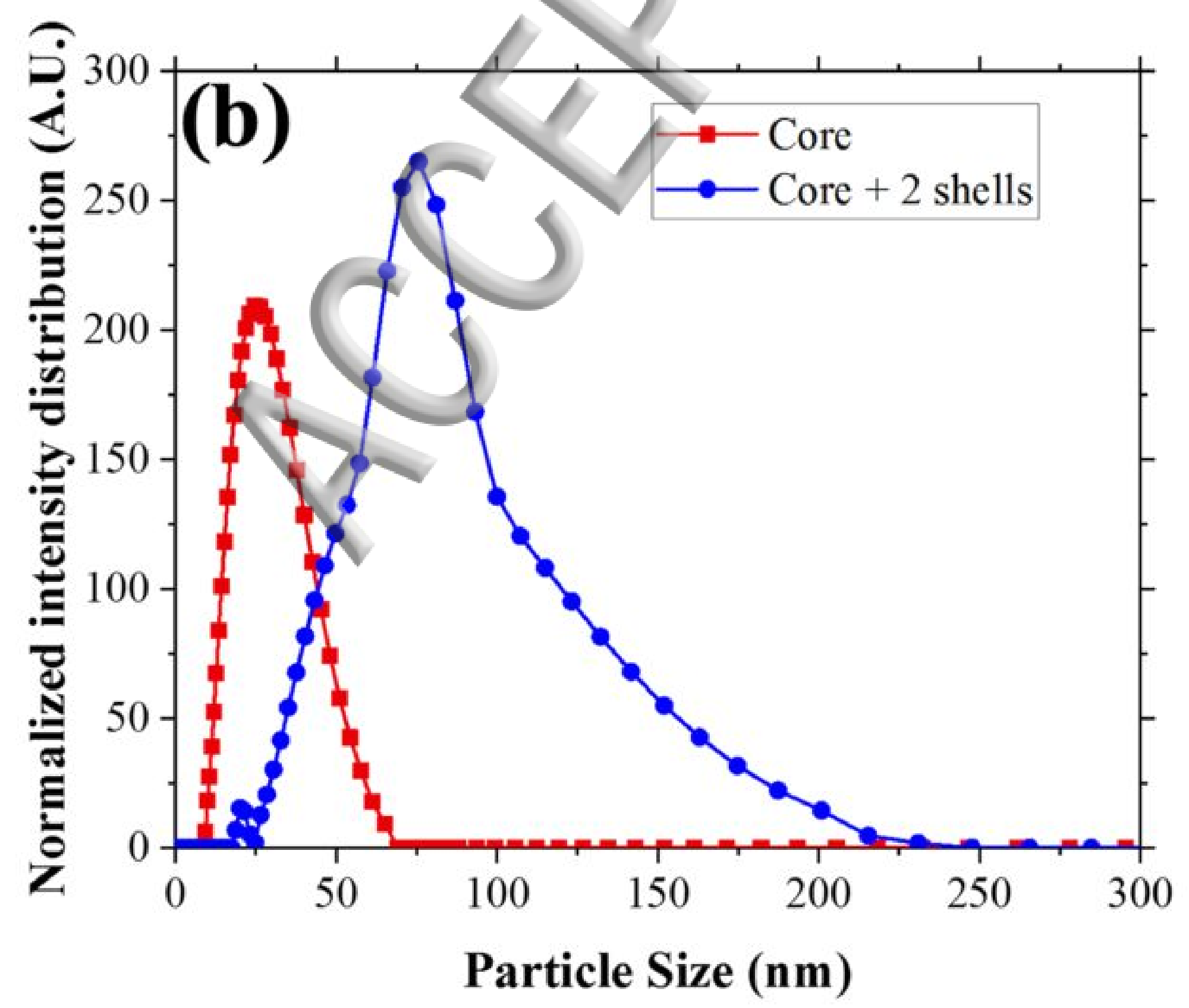
(b)
Core
Core + 2 shells
Normalized intensity distribution (A.U.)
Particle Size (nm)
0
50
100
150
200
250
300

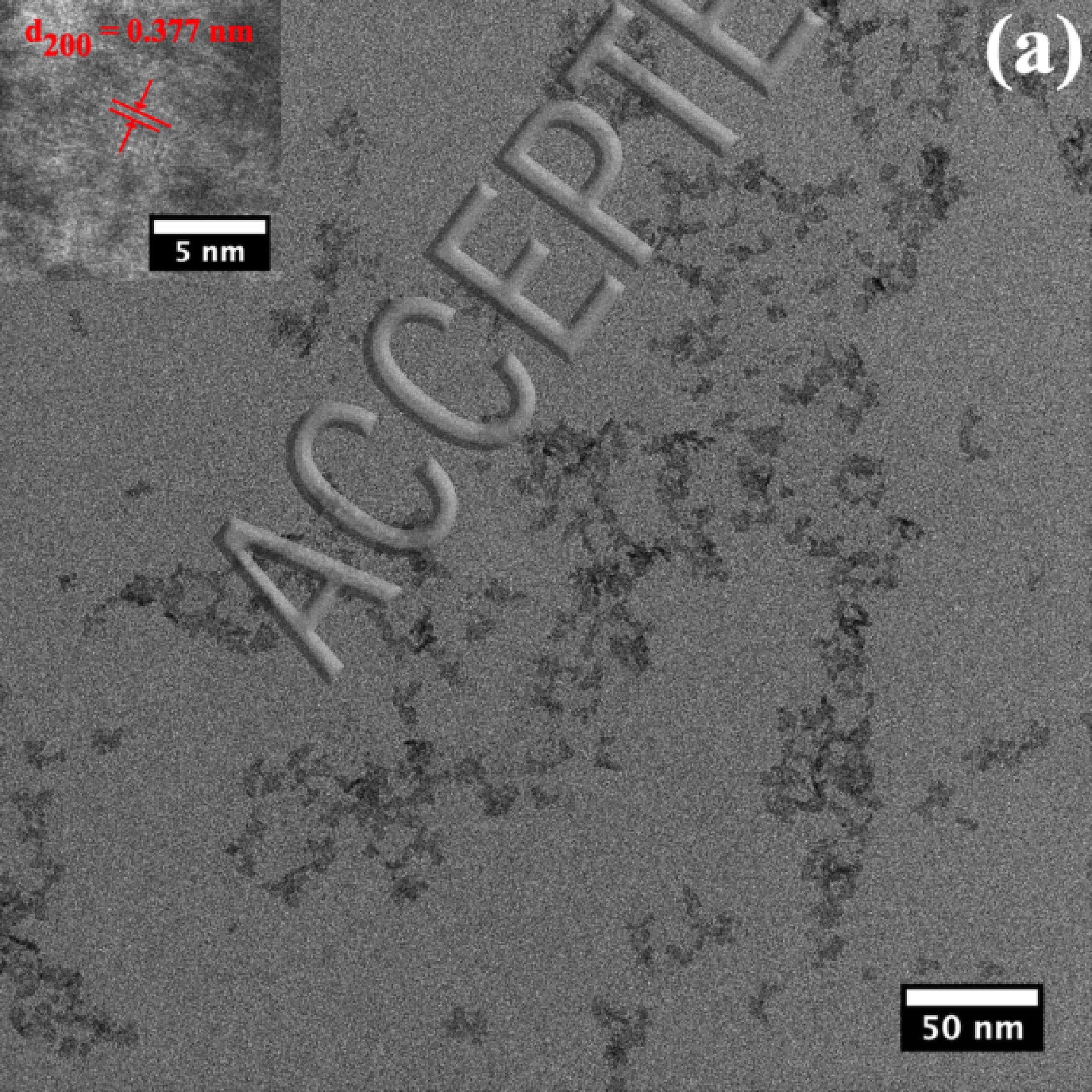
d_{200} = 0.377 nm
5 nm
(a)
ACCEPTED
50 nm

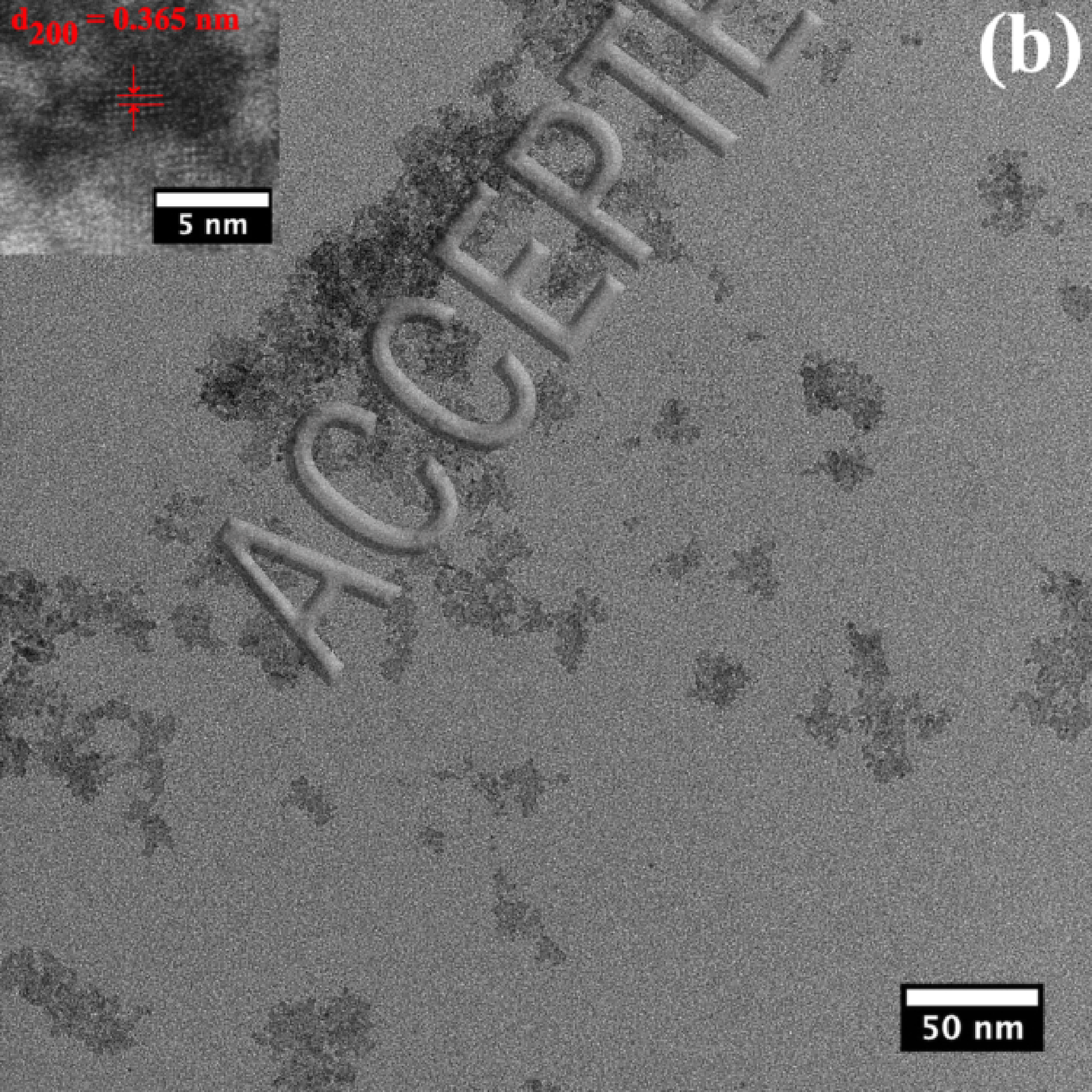
d_{200} = 0.365 nm
5 nm
(b)
ACCEPTED
50 nm

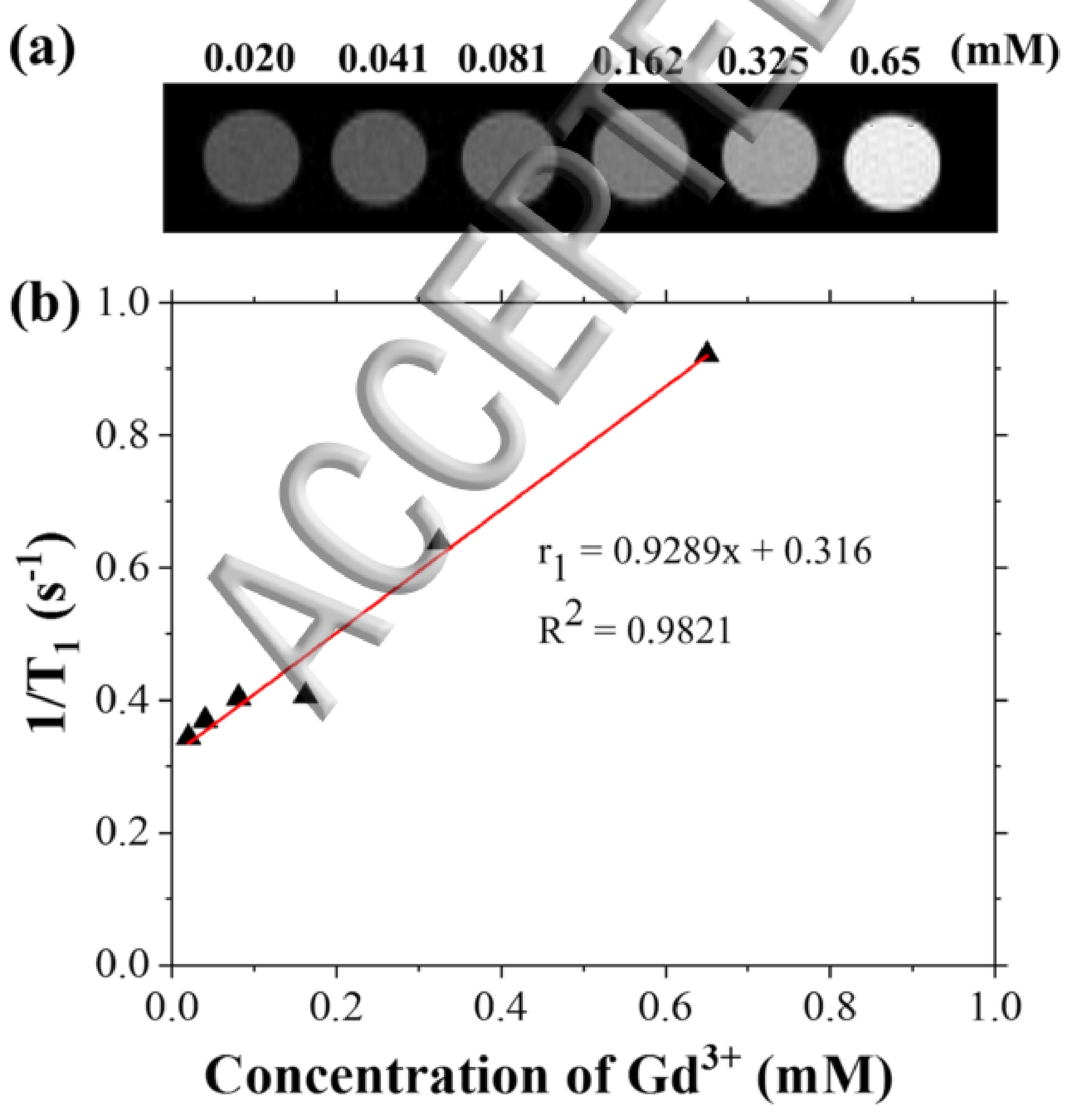
(a)
0.020
0.041
0.081
0.162
0.325
0.65
(mM)
(b)
1.0
0.8
0.6
0.4
0.2
0.0
1/T1 (s-1)
r1 = 0.9289x + 0.316
R2 = 0.9821
0.0
0.2
0.4
0.6
0.8
1.0
Concentration of Gd3+ (mM)

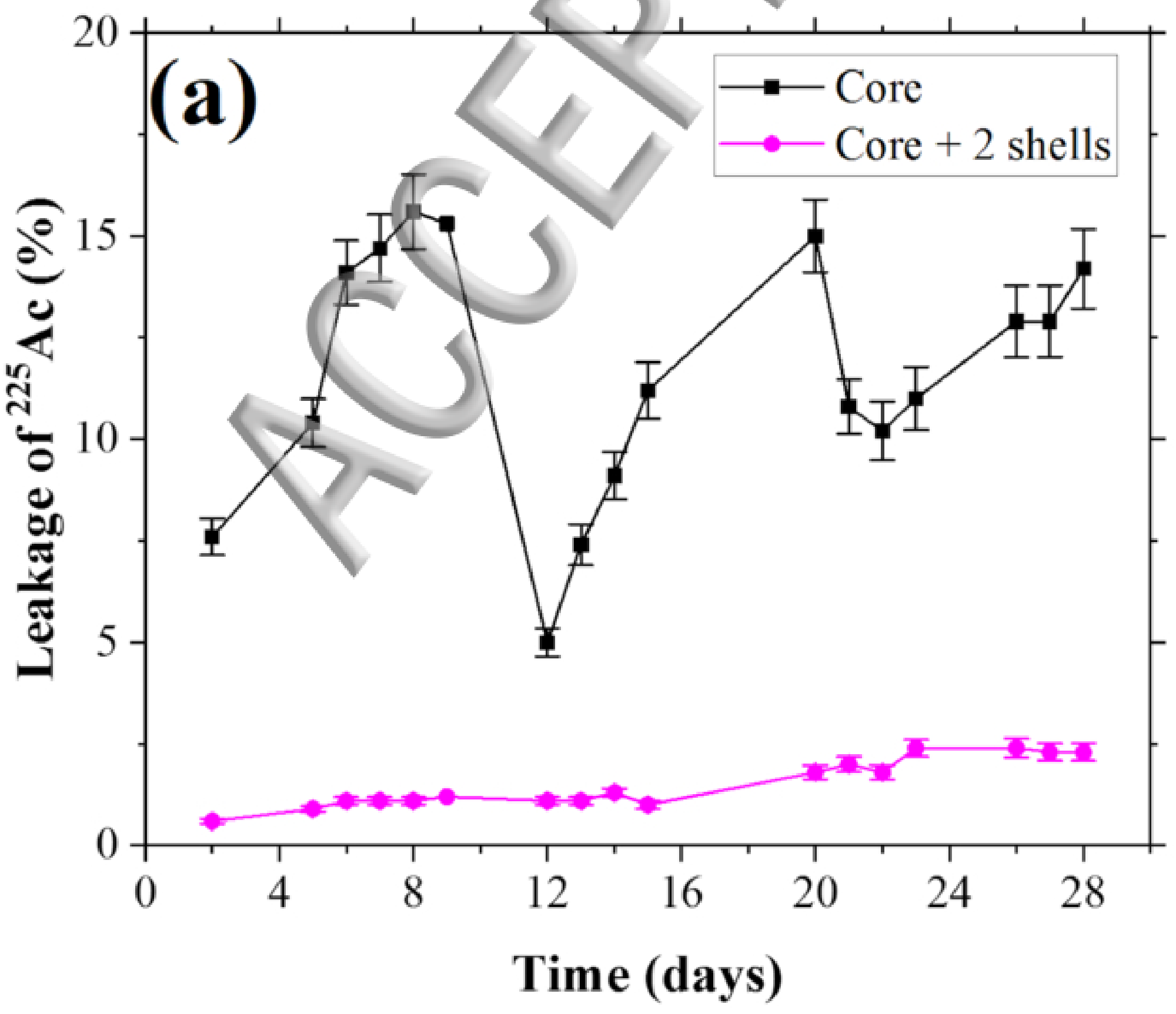
(a)
Core
Core + 2 shells
Leakage of ^{225}Ac (%)
Time (days)
0
5
10
15
20
0
4
8
12
16
20
24
28

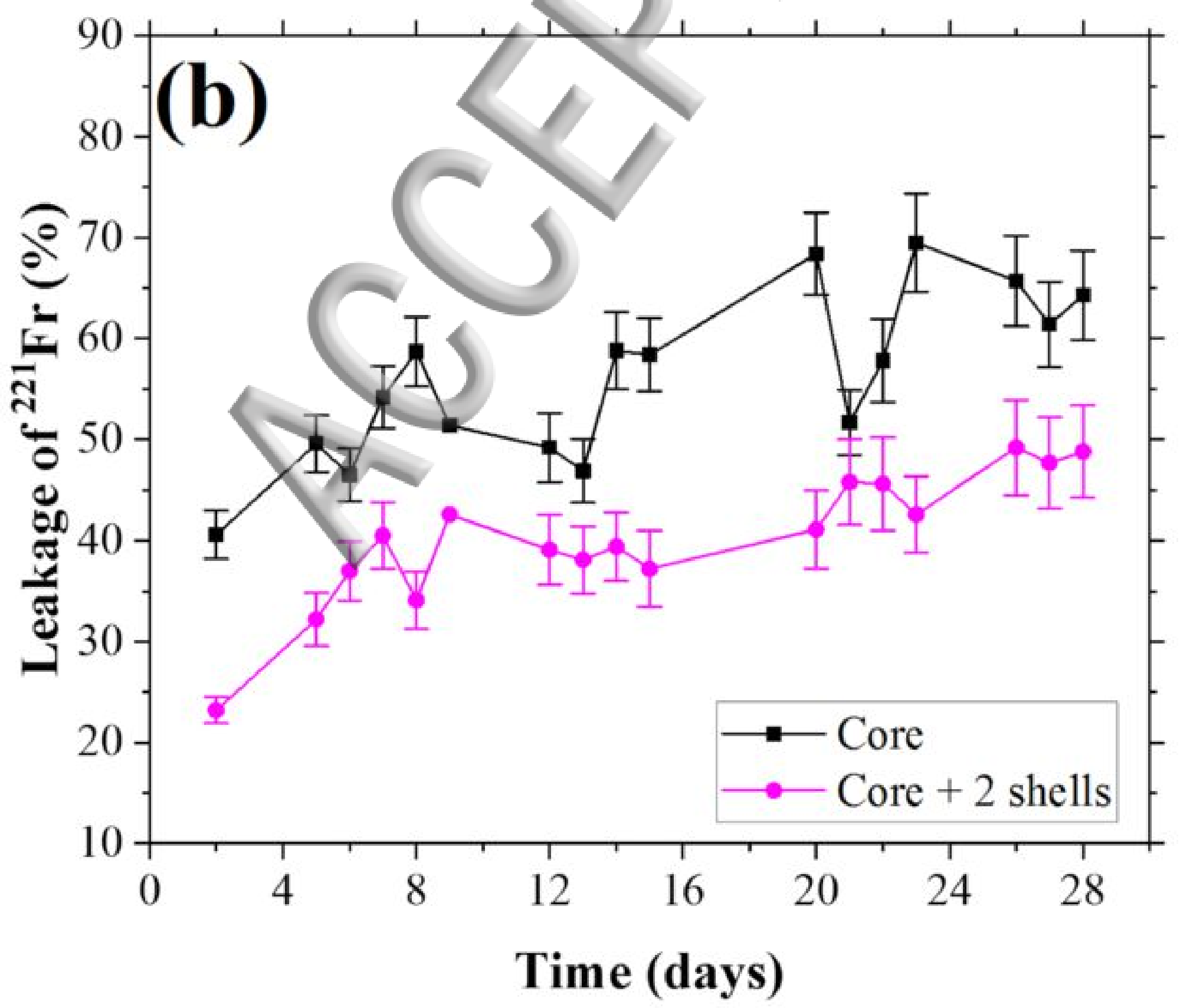
(b)
Leakage of ^{221}Fr (%)
Time (days)
Core
Core + 2 shells
90
80
70
60
50
40
30
20
10
0
4
8
12
16
20
24
28

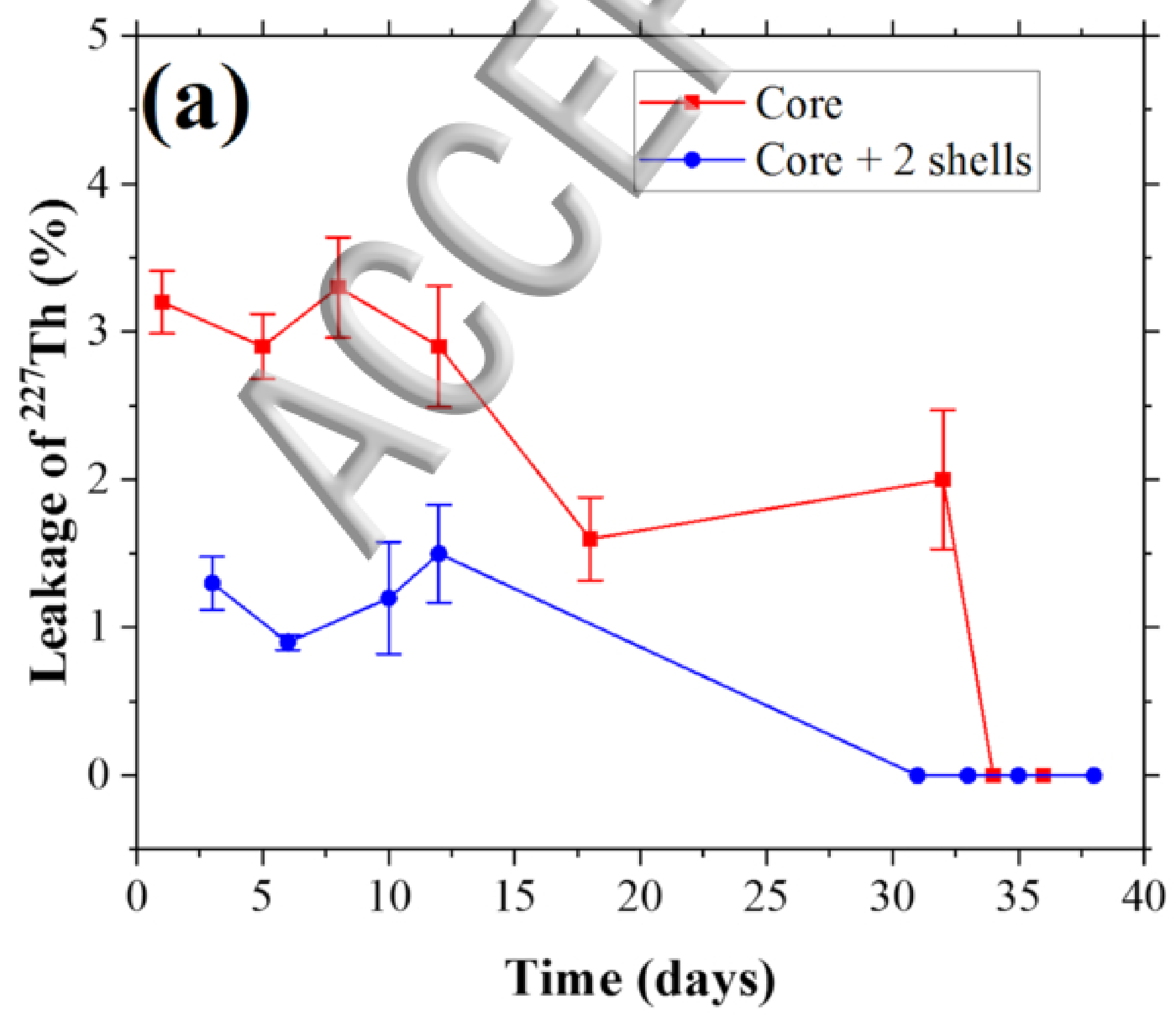
(a)
Core
Core + 2 shells
Leakage of ^{227}Th (%)
Time (days)
0
1
2
3
4
5
0
5
10
15
20
25
30
35
40

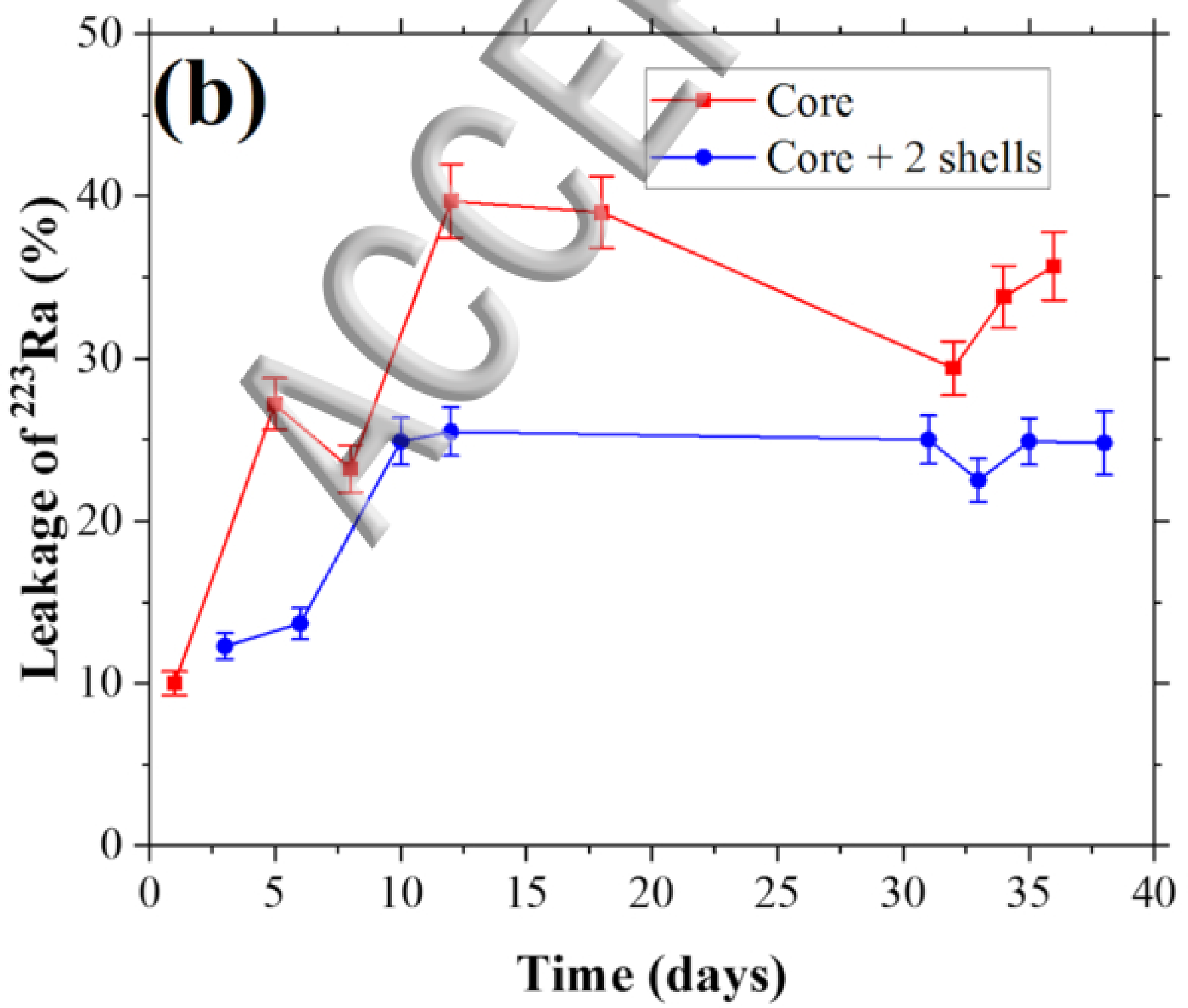
(b)
Core
Core + 2 shells
Leakage of ^{223}Ra (%)
Time (days)
0
10
20
30
40
50
0
5
10
15
20
25
30
35
40